KfK 5179
August 1994

Compatibility of Graphite with a Martensitic-Ferritic Steel, an Austenitic Stainless Steel and a Ni-Base Alloy up to 1250°C

P. Hofmann, M. Markiewicz
Institut für Materialforschung
Projekt Kernfusion

Kernforschungszentrum Karlsruhe

Kernforschungszentrum Karlsruhe
Institut für Materialforschung
Projekt Kernfusion

KfK 5179

Compatibility of Graphite with a Martensitic-Ferritic Steel, an Austenitic Stainless Steel and a Ni-Base Alloy up to 1250°C

P. Hofmann, M. Markiewicz*

*Comisión Nacional de Energia Atómica
Av. del Libertador 8250, 1429 Buenos Aires
Argentina

Kernforschungszentrum Karlsruhe GmbH, Karlsruhe

Kernforschungszentrum Karlsruhe GmbH
Postfach 3640, 76021 Karlsruhe

ISSN 0303-4003

Abstract

To study the chemical interactions between graphite and a martensitic-ferritic steel (1.4914), an austenitic stainless steel (1.4919; AISI 316), and a Ni-base alloy (Hastelloy X) isothermal reaction experiments were performed in the temperature range between 900 and 1250°C. At higher temperatures a rapid and complete liquefaction of the components occurred as a result of eutectic interactions.

The chemical interactions are diffusion-controlled processes and can be described by parabolic rate laws. The reaction behavior of the two steels is very similar. The chemical interactions of the steels with graphite are much faster above 1100°C than those for the Ni-base alloy. Below 1000°C the effect is opposite.

Verträglichkeitsverhalten von Graphit und einem martensitisch-ferritischen Stahl, einem austenitischen Stahl und einer Ni-Basislegierung bis 1250°C

Kurzfassung

Zum Studium des Verträglichkeitsverhaltens von Graphit gegenüber einem martensitisch-ferritischen Stahl (1.4914), einem austenitischen Stahl (1.4919) und einer Nickelbasislegierung (Hastelloy X) wurden isotherme Reaktionsglühungen im Temperaturbereich von 900 bis 1250°C durchgeführt. Bei höheren Temperaturen fand eine schnelle und vollständige Verflüssigung der Komponenten infolge eutektischer Wechselwirkungen statt.

Die chemischen Wechselwirkungen sind diffusionskontrollierte Prozesse und können durch parabolische Zeitgesetze beschrieben werden. Das Verträglichkeitsverhalten des martensitisch-ferritischen und des austenitischen Stahles ist gegenüber Graphit vergleichbar. Oberhalb 1100°C verlaufen die chemischen Wechselwirkungen zwischen Graphit und den beiden Stählen deutlich schneller als bei der untersuchten Nickelbasislegierung. Unterhalb 1000°C ist das Reaktionsverhalten gerade umgekehrt.

Contents

1. Introduction

The first wall of a fusion reactor is the first solid barrier between the plasma and the outside of the reactor. It has to be protected against plasma disruptions or discharges of runaway electrons. One of the protection materials considered has been pure fine grained graphite (C) or carbon fibre carbon composite (CFC) material. The operation temperature of the protection tiles can be far above 1000°C. Component tests are required to study the physico-chemical behavior of the first wall materials in case of solid contact under normal and abnormal operating conditions or in accidents (in case of failure of the cooling system of the support structure).

For the first wall itself metallic materials have been used or are under consideration : nickel-base alloys, austenitic stainless steels, and martensitic-ferritic steels. For this reason, the compatibility of these three metallic materials with carbon (graphite) at elevated temperatures has been examined.

2. Experimental Details

The isothermal annealing tests were performed with the metallic materials 1.4919 (AISI 316) austenitic stainless steel, 1.4914 martensitic-ferritic steel and the Ni-base alloy Hastelloy X as capsules filled with C (graphite) powder. The nominal chemical compositions of the 1.4919 austenitic stainless steel, 1.4914 martensitic-ferritic steel and Hastelloy X are indicated in Table 1. Three material couples were tested. To obtain a good solid-state contact between the graphite powder and the capsule wall, the powder was pressed into the crucible-shaped capsules. After that, the capsules were closed gastight by conical plugs. The specimens were prepared and sealed in a glovebox under inert gas conditions. Figure 1 shows schematically the annealing capsules.

The annealing experiments were performed in a tube furnace under flowing argon. The temperature ranges investigated for the three reaction couples varied between 900 and 1250°C. The annealing time ranged from 5 minutes to 400 hours. The maximum temperature of 1250°C was limited by the onset of liquid phase formation and the subsequent fast and complete liquefaction of the specimens at slightly higher temperatures. At lower temperatures the interactions are very slow.

After annealing the specimens were mechanically cut and then metallographically prepared for examinations of the reaction zones with an optical

microscope. The thicknesses of the reaction zones were measured at four different locations of the powder/metal interface. In addition, Scanning Electron Microscopy (SEM)/Energy Dispersive X-Ray (EDX) and Auger Electron Spectroscopy (AES) examinations were made to obtain information on the chemical composition of the reaction products and diffusion zones.

3. Results

The analysis of the results of isothermal capsule tests is focused mainly on in the determination of the reaction kinetics, the identification of the reaction species, and the phases formed due to the chemical interactions of the material couples examined.

3.1 Chemical behavior

3.1.1 Chemical interactions of C (graphite) with 1.4914 martensitic-ferritic steel and 1.4919 austenitic stainless steel

The chemical interactions between C and 1.4914 ferritic steel and 1.4919 stainless steel, respectively, resulted in the formation of two reaction layers on the inner surface of the annealing capsules. The reaction layer I, adjacent to graphite, was thinner and can be characterized by a volume attack with a rather homogeneous appearance. The reaction layer II is a transition zone located between the reaction layer I and the unattacked steel matrix; it is much thicker and can be characterized by a great amount of precipitations within the grains and at the grain boundaries. Figure 2 shows the reaction zones in the C/1.4914 ferritic steel system for specimens annealed at different temperatures and times. Although the two reaction layers were observed at all temperatures and times examined, the morphology of the reaction layer I changes noticeably at temperatures of 1200°C and above. The onset of eutectic melting takes place at some locations and produces numerous macrovoids as a result of partial melting and relocation of the liquid alloy.

The liquid phase formation can be explained by binary and ternary phase diagram considerations. The (C-Cr) and (C-Ni) phase diagrams show eutectic interactions in each system, Figures 3, 4 [1, 2]. The eutectic temperatures are lowest in the (C-Fe) system at about 1150°C on the Fe-rich side. The diffusion of approximately 4 wt. % C into Fe results in the formation of a liquid phase even at this low temperature. The eutectic temperature in the (C-Ni) system is about 1326°C while the lowest eutectic temperature in the system (C-Cr) is around

1534°C. The liquid phase formation, as experimentally observed, is also predicted by the liquid projection diagram of the ternary (Fe-Cr-C) system, Figure 5 [3]. The solid thick curves are the liquid field boundaries of the primary crystals: the arrows along these boundaries indicate their direction with decreasing temperature. The liquid surface defined by the isothermal contour at 1200°C is crossed by the connecting (tie) line x-y, which represents as a first approximation the initial C/1.4914 ferritic steel reaction system. Since the steel also contains small amounts of Ni, Mo, Mn, some changes in the onset of liquid phase formation have to be expected.

The reaction zones in the specimens were examined by Auger Electron Spectroscopy. Besides the determination of the distribution of the elements, quantitative measurements were performed to obtain the chemical compositions of the various phases. Typical results for a C/1914 steel diffusion couple annealed at 1250°C for 5 min are shown in Figure 6. As can be recognized, the reaction layer I consists mainly of an (Fe, Cr) carbide phase distributed in a modified Cr-free steel matrix. The integral chemical analysis of the reaction layer I, liquid at temperatures $T \geq 1200°C$ yields the following values: about 81 wt. % Fe, 9 wt. % Cr, 7 wt.% C. The black square in Figure 5 indicates the compositon of the alloy in the (C-Cr-Fe) liquid surface; which is very close to the tie line x-y.

The microstructure of the solidified alloy can be predicted from the ternary (C-Cr-Fe) liquid projection diagram (Figure 5). During cooldown, the liquid alloy situated on the right joint U_5-P_1 dictates that freezing commences by the precipitation of C (graphite), Figure 6, lowering the carbon content of the liquid toward the joint U_5-P_1 whereupon $(Fe, Cr)_7C_3$ crystals start to form at the expense of graphite and liquid according to the reaction $L \leftrightarrows C\ (Fe,Cr)_7C_3$. The crystallization of $(Fe,Cr)_7C_3$ moves the liquid composition to point P_1 where the reaction $L + C + (Fe,Cr)_7C_3 \leftrightarrows (Fe, Cr)_3C$ leads to the formation of a shell of $(Fe, Cr)_3C$ around the initially formed $(Fe, Cr)_7C_3$ phase, like a peritectic reaction. With decreasing temperature, the composition of the liquid moves from P_1 to U_3, the reaction $L + (Fe,Cr)_7C_3 \leftrightarrows (Fe,Cr)_3C$ reduces to a certain extent the $(Fe,Cr)_7C_3$ crystal moving the liquid down to point U_3, the remaining liquid solidifies in the eutectic reaction $L \leftrightarrows (Fe,Cr)_3 + \gamma$ Fe. The formation of a duplex carbide, consisting of cores of $(Fe,Cr)_7C_3$ surrounded by shells of $(Fe,Cr)_3C$, predicted by the liquid projection, is observed in the microstructure of Figure 7. Similar observations were made in references [4 and 5] for different cooling rates.

Microhardness measurements were performed on the duplex carbide; a microhardness of 1705 kg/mm^2 was measured for (Fe, Cr)$_7$C$_3$ and 980 kg/mm^2 for the compound (Fe, Cr)$_3$C, the literature [6, 7] gives 1735 and 1035 kg/mm^2, respectively, for the same compounds. The microhardness results support the quantitative chemical results for the two observed M_7C_3 and M_3C compounds.

In the experiments performed at the lower temperatures of 900, 1000 and 1100°C, no liquid phase formation was observed. The chemical analysis of the reaction layer I shows that this layer consists of a metal carbide of the chemical form "MC" with the following chemical composition: about 55 wt. % Fe, 27 wt. % Cr and 18 wt. % C and a Cr depleted zone. Figure 8 shows the reaction zones and the distribution of Cr and C of a C/1.4914 ferritic steel reaction couple annealed at 1000°C for 100 h. Next to the Cr depleted zone within the reaction layer I, a zone with many carbide precipitations forms in the steel matrix. It will be shown in Chapter 3.2 that this Cr depleted zone, caused by the (Fe Cr) carbide formation, limits the growth of the reaction layer I due to the reduced availability of Cr to form a sTable (Fe, Cr) carbide.

The (Cr, Fe) carbide precipitations within the grains and at the grain boundaries in the reaction layer II have the same chemical compositions, about 55 wt. % Cr, 23 wt. % Fe, 10 wt. % Mo and 12 wt. % C, identified as compound M_3C_2 which is different from that of the carbide layer of reaction zone I . The amount of these (Cr, Fe, Mo) carbide precipitations decreases with increasing distance from the C/steel interface.

In spite of the difference in chemical compositions between the 1.4914 martensitic-ferritic steel and the 1.4919 austenitic stainless steel (see Table 1), the reaction behavior with respect to graphite is similar. In the different reaction zones the same diffusing species, reaction layers and carbide phases were found . Figures 9 and 10 show the metallographic appearance of the reaction zones in the system C/1.4919 stainless steel for specimens annealed at different temperatures and times. The reason for this behavior may be the reduced affinity of Ni for carbon compared with that for Cr and Fe, and the low solubility of Ni in the carbide phases. The same effect has been found in boride phases [8].

3.1.2 Chemical interactions between C (graphite) and the Ni-base alloy Hastelloy X

The structure of the reaction zone in the C/Hastelloy X chemical interactions is strongly influenced by the temperature at which the experiments were performed. The changes in the microstructure are determined by the liquid phase formation at temperatures of about 1250°C and above as a consequence of eutectic interactions. Figures 11 and 12 show typical examples of reaction zones for specimens annealed at 1100 and 1250°C. The reaction zones were similar for all temperatures below 1200°C and are characterized by the formation of two or three interfacial reaction layers; a typical result of microstructure and chemical composition measurements on a specimen annealed at 1100°C for 49 h is shown in Figure 13. Within the volume attack zone I, the formation of a metal carbide layer, adjacent to the graphite, and a Cr-depleted layer (precipitation-free zone) caused by the preferential diffusion of Cr toward the graphite side, can be recognized. The reaction zone II consists in addition of a layer with carbide precipitations within the grains and at the grain boundaries of the Hastelloy matrix.

The chemical analysis of the reaction zone shows that the reaction layer adjacent to the graphite is a Cr-base carbide with the following chemical composition: about 60 wt. % Cr, 12 wt. % Fe, 6 wt. % Mo, 4 wt. % Ni and 18wt. % C, referred to as MC carbide. The enrichment of chromium suggests that chromium is the preferential reacting species, which governs the growth of this reaction layer. The Cr-base carbide precipitates within the grain and at the grain boundaries have different chemical composition, about 56 wt. % Cr, 20 wt. % Mo, 7 w. % Fe, 4 wt. % Ni and 13 wt. % C, referred as M_3C_2; the same morphology, distribution and compositon was observed at all temperatures. At temperatures of 1250°C evidence of eutectic melting appears within the volume attack zone, which increases the reaction zone growth rate. Figure 14 shows the microstructure and chemical composition of the solidified reaction zone (adjacent to graphite), and the carbide precipitation layer (next to the non-attacked Hastelloy X matrix), for a specimen annealed at 1250 °C for 15 min. The integral chemical composition of the solidified reaction zone indicates the following values: about 44 wt. % Ni, 19.3 wt. % Fe, 18.4 wt. % Cr, 9.2 wt. % C, and 9.1 wt. % Mo.

The information of the available binary and ternary phase diagrams can be used to a limited extent only; however, eutectic melting could be explained on the

basis of the liquid projection diagram for the (C-Fe-Ni) system, Figure 15 [9]; the lowest eutectic temperature in the eutectic valley e_1-e_2 is 1125°C at 20 wt. % Ni, rising to 1168°C at 30 wt. % Ni. The higher nickel content of Hastelloy X (47 wt %) raises even more the melting temperature of the (C-Fe-Ni) system. The liquid phase formation at around 1250°C, as experimentally observed, seems to be reasonable. No other (C-Ni-M) system (M=Cr, Mo) shows a liquid phase-formation at these low temperatures. Therefore, as shown in the C/steel interactions, the (Fe-C) eutectic interaction seems to initiate melting of the reaction zone.

Many phases develop during solidification; the structure consists of primary graphite flakes (black areas in Figure 14), secondary crystals of Cr-base carbide with a chemical compositon of about 51 wt. % Cr, 13 wt. % Fe, 11 wt. % Mo, 8 wt. % Ni and 16 wt. % C (referred to as MC), and a transformed matrix with a high Ni content; the eutectic microstructure is evident in Figures 12 and 14. The results show that the temperature of liquid phase formation of around 1250 °C, due to the C/Hastelloy X chemical interaction is not far away from the incipient melting temperature of Hastelloy X, 1260°C, with a melting range between 1260 and 1355 °C [10].

3.3 Reaction kinetics

To determine the reaction kinetics of the reaction couples tested, the reaction zone thicknesses of the reaction layers (volume attack and total reaction zone) were measured as a function of the annealing time in the temperature range of 900 - 1250 °C. The results are listed in Tables 2, 5 and 8 and plotted in Figures 16 through 22 for the three systems examined. The isothermal growth of the reacting layer thickness is a linear function of the square root of time (parabolic rate law) in the whole range of temperatures. This is an indication of a diffusion-controlled chemical interaction. The calculated growth rates of the reaction zone for the diffusion couples C/1.4914 ferritic steel, C/1.4919 stainless steel and C/Hastelloy X are listed in Table 3, 6 and 9, respectively, and are plotted in the same order versus the reciprocal temperature in Figures 23, 24 and 25. The determined equations of growth rates and the validity of their temperature range are indicated in Tables 4, 7 and 10. All the Tables and Figures represent the results of measurements made with an optical light microscope during the metallographic examinations. The following remarks can be made concerning the different systems:

3.3.1 C/1.4914 martensitic-ferritic steel system:

- It was not possible to determine the depth of the total reaction zone at temperatures below 1200°C due to the uncertainty in defining the real phase boundary at which the precipitation population had reached the level of the control specimen (control specimen: same annealing conditions but without graphite).

- The only data obtained correspond to the volume attack. It is not possible to compare the total reaction depth with the other steel or Hastelloy X.

- Considering the volume attack, it was observed that at 1100°C the reaction was slower than at 1000°C. ((Figure 16) similar to C/1,4919 (Figure 18)).

- The drastic change in the activation energy at 1200°C to a much higher value may be explained by eutectic melting within the volume attack layer. Liquefaction of the specimens takes place above 1250°C.

3.3.2 C/1.4919 austenitic stainless steel system:

- Only above 1100°C could the total reaction depth be precisely determined. At lower temperatures it was not possible to detemine the real phase boundary at which the precipitations had reached the level of the control specimen.

- Below 1100°C the limit of the precipitation zone was postulated to be that given by C tracer diffusion into stainless steel (AISI 316 L).

- Recrystallization of the steel (1000 - 1100°C) seems to have stopped the advance of the precipitation zone into the steel. Between 1000 and 1100°C the growth rate of the total reaction zone decreases.

- The change in the activation energy at temperatures above 1100°C can be attributed to the liquid phase formation. Eutectic melting was observed at 1200°C within the volume attack zone. The diffusion couple liquefies above 1250°C.

3.3.3 C/Hastelloy X system:

- The total reaction depth could be precisely determined only at temperatures of 1200 and 1250°C, for the same reason as explained for the previous systems.

- At 1250°C there is a strong increase in the reaction rate, with evidence of eutectic melting appearing just at 1250°C within the volume attack zone.

The growth rate equations determined for the different systems cannot be extrapolated to higher temperatures. At temperatures slightly higher than 1250°C the reaction specimens became completely liquefied within a few seconds as a result of eutectic interactions.

4. Discussion

The chemical interactions of C (graphite powder) with 1.4914 ferritic steel, 1.4919 stainless steel and Hastelloy X can be described by parabolic rate laws for the temperature range of 1000 - 1250°C, i. e. diffusion processes are the rate determining steps. To describe the chemical reaction in the three different systems, two Arrhenius equations are necessary. The change to higher values in the activation energy of the Arrhenius equation is caused by the formation of liquid phases which accelerate the extent of interaction, resulting in complete liquefaction of the reaction couple above 1250°C. Figure 26 shows the pronounced temperature sensitivity of the reaction above 1100°C for the C/stainless steel couple and above 1200°C for the couple C/Hastelloy X. In the case of the C/stainless steel reaction systems, the chemical interactions above 1100°C are much faster than in the C/Hastelloy X reaction system by about two orders of magnitude. Below 1000°C the chemical compatibility between C and Hastelloy X seems to be superior.

The chemical interactions of C with 1.4914 ferritic steel and 1.4919 stainless steel do not show a marked difference in the reaction growth rate in the range of temperatures examined; also, the same reaction species and phases were found in the reaction zones. The different chemical compositions of the steels examined probably play a minor role only. The growth of the reaction layer I (adjacent to graphite) is presumed to be governed by the interdiffusion of C, Fe and Cr, to form Fe-base carbides. Carbon diffuses rapidly into the steel or Hastelloy, most of the chromium reacts with carbon in the alloy matrix to form Cr base carbides. In the case of the chemical interaction between C and Hastelloy X, C and Cr seem to

be the preferred reaction species to form Cr-base carbides in the reaction layer I and in the Hastelloy matrix. The data of the preferential diffusion species in the reaction layers are necessary to be able to take into account the details of the reaction mechanisms.

The (Fe, Cr) carbide reaction layers also play an important role with respect to the critical upper temperature at which the liquid phase forms as a result of eutectic interactions. At temperatures slightly higher than 1250°C fast and complete liquefaction of the reaction couples takes place. The ternary (C-Fe-Cr) and (C-Fe-Ni) liquid projection diagrams give a reasonable explanation of the low-temperature liquefaction for the C/stainless steel and C/Hastelloy X systems, respectively, Figures 5 and 15. The lowest eutectic temperature of the Fe-Fe_3C subsystem at about 1150°C, (Figure 3) seems to be the cause of the first liquid phase formation at about 1200°C, as experimentally observed for the C/stainless steel system and at 1250°C for the C/Hastelloy X system. These failure temperatures are by about 250°C lower than the melting point of stainless steel and about by 100°C lower than that of Hastelloy X.

5. Summary and Conclusions

The growth kinetics of reaction layers, the reaction products and the structure of the reaction zones in the C/1.4914 martensitic-ferritic steel, C/1.4919 austenitic stainless steel and C/Hastelloy X systems were studied at temperatures ranging from 900 to 1250°C. The results of the chemical interactions can be summarized as follows:

- C (graphite) in contact with stainless steel or Hastelloy X gives rise to chemical interactions which can be described by parabolic rate laws, which means that they are diffusion-controlled processes.

- The reaction kinetics become very rapid above 1100°C for the C/stainless steels (1.4914, 1.4919) reaction couple and above 1200°C for the C/Hastelloy X reaction couple. The increase in the activation energy is caused by liquid phase formation.

- In the three reaction systems examined liquefaction occurs below the melting point of the components due to eutectic interactions. Beyond 1250°C fast and complete liquefaction of the compatibility specimens takes place.

- The chemical interactions above 1100°C are much faster for the C/stainless steels than for C/Hastelloy X. Below 1000°C the effect is opposite.
- The low-temperature liquid phase formation in the three systems examined is asociated with (Fe-C) eutectic interaction.

6. Acknowledgements

We thank Prof. Dr. W. Dienst (KfK, Germany) and Dr. T. Haste (AEA Technology, UK) for the critical reading of the paper and their valuable comments.

7. References

[1] T. B. Massalski; Binary Alloy Phase Diagrams, Vol. 1, American Society for Metals, 2nd Edition (1986).

[2] Bulletin of Alloy Phase Diagrams, Vol. 11, No. 2, p. 152, (1990).

[3] V. G. Rivling: Critical review of the constitution of (C-Cr-Fe) and (C-Fe-Mn) systems, International Metals Reviews, (1984), Vol. 29, No. 4, p. 299.

[4] N. R. Griffing, W. D. Forgeng, G. W. Healy: (C-Cr-Fe) Liquidus Surface, Transaction of the Metallurgical Society of AIME, Vol 224, p. 148, (1962).

[5] G. Laird, R. L. Nielsen, N. H. Macmillan: On the nature of eutectic carbides in Cr-Ni white cast irons, Metallurgical Transactions A, Vol. 22 A, p. 1709, (1991).

[6] R. B. Gundlach, J. L. Parks: Wear, (1978), Vol. 46, pp. 97 - 108.

[7] G. L. Powell: Met. Forum, 1980, Vol. 3, pp. 37 - 46.

[8] S. Ihara, K. Tanaka, M. Kojima, Y. Akimoto: IAEA-IWGFR Specialist Meeting on Development and Applications of Absorber Materials, Dimitrovgrad, USSR, June 3 - 8, (1973), pp. 201 - 228.

[9] V. G. Rivling: Review of the constitution of (C-Fe-X) systems, International Metals Reviews, (1984), Vol. 29, No. 2, p. 104.

[10] Metals Handbook, Tenth Edition, Vol. 1, p. 963, (1988)

List of Tables

List of Figures

Table 1: Chemical compositons of 1.4914 ferritic steel, 1.4919 stainless steel and Hastelloy X (in wt. %)

Element	1.4914	1.4919	Hastelloy X
Ni	1.2	14	47.4
Cr	12	18	21.6
Fe	83.6	63	18.8
Mo	1	2.5	9
Si	0.6	0.8	0.2
Mn	1.3	2	0.8
C	0.2	0.1	0.1
Co	-	-	1.5

Table 2: Measured reaction zone thickness for the C/ferritic steel 1.4914 diffusion couple as a function of temperature and time

Specimen	Temperature °C	Time h	Measured reaction zone thickness, µm	
			I	II
813	900	25	13	-
814	900	100	33	
815	900	400	64	
817	1000	25	55	-
816	1000	100	93	
818	1000	225	118	
820	1100	6	15	-
819	1100	25	12	
821	1100	49	30	
822	1200	0.083	1460	1900
824	1200	0.167	1600	2200
823	1200	0.25	1000	1700
887	1250	0.083	900	-
888	1250	0.167	1660	

I - volume attack (includes precipitation-free zone, except at 1100°C)
II - total reaction zone.

Table 3: Reaction zone growth rates for the C/ferritic steel 1.4914 diffusion couple as a function of temperature (900 - 1250°C)

Temperature [°C]	Reaction zone growth rate, x^2/t^*, cm^2/sec	
	I	II
900	$2.81 \cdot 10^{-11}$	-
1000	$2.02 \cdot 10^{-10}$	-
1100	$4.10 \cdot 10^{-11}$	-
1200	$2.73 \cdot 10^{-5}$	$5.81 \cdot 10^{-5}$

I - volume attack
II - total reaction zone

* values adjusted by linear regression from kinetic data at constant temperature

Table 4: Growth rate equations for the C/ferritic steel 1.4914 interactions

Phenomena	Temperature range, °C	Growth rate equation, x^2/t, cm^2/s
Volume attack (I)	900 - 1100	$1.225 \cdot 10^{-9} \exp(-31516/RT)$
Volume attack (I)	1100 - 1250	$4.55 \cdot 10^{71} \exp(-2149518/RT)$

R = 8.314 J/mol K

Table 5: Measured reaction zone thickness for the C/stainless steel 1.4919 diffusion couple as a function of temperature and time

Specimen	Temperature° C°	Time h	Measured reaction zone thickness, µm	
			I	II
841	900	25	21	-
842	900	100	38	
843	900	400	60	
845	1000	25	25	-
846	1000	49	50	
844	1000	100	57	
848	1100	6	5	
847	1100	25	25	
849	1100	49	45	400
850	1200	0.08	1106	1275
852	1200	0.17	958	1168
851	1200	0.25	1047	1237
891	1250	0.08	1910	2185
892	1250	0.17	3000	3300

I - volume attack (includes precipitation-free zone, except at 1100°C)
II - total reaction zone.

Table 6: Reaction zone growth rates for the C/stainless steel 1.4919 (AISI 316) diffusion couple as a function of temperature (900 - 1250°C)

Temperature °C	Reaction zone growth rate, x^2/t^*, cm^2/s	
	I	II
900	$2.81 \cdot 10^{-11}$	-
1000	$1.0 \cdot 10^{-10}$	-
1100	$8.88 \cdot 10^{-11}$	$9.07 \cdot 10^{-9}$
1200	$1.67 \cdot 10^{-5}$	$2.35 \cdot 10^{-5}$
1250	$1.38 \cdot 10^{-4}$	$1.71 \cdot 10^{-4}$

I - volume attack
II - total reaction zone

* Values adjusted by linear regression from kinetic data at constant temperature
** Single or averaged values (without linear regression analysis)

Table 7: Growth rate equations for the C/stainless steel 1.4919 (AISSI 316) interactions

Phenomena	Temperature range, °C	Growth rate equation, x^2/t, cm^2/s
Volume attack (I)	900 - 1100	$1.14 \cdot 10^{-7} \exp(-79039/RT)$
Volume attack (I)	1100 - 1250	$1.30 \cdot 10^{56} \exp(-1734701/RT)$
Total reaction zone (II)	1100 - 1250	$1.08 \cdot 10^{37} \exp(-1182954/RT)$

R = 8.314 J/mol K

Table 8: Measured reaction zone thickness for the C/Hastelloy X diffusion couple as a function of temperature and time

Specimen	Temperature °C	Time h	Measured reaction zone thickness, μm	
			I	II
869	900	25	8	across the
870	900	100	13	whole
871	900	400	22	sample
873	1000	25	25	-
872	1000	100	48	
874	1000	225	68	
875	1100	6	37	-
876	1100	25	53	
877	1100	49	98	
878	1200	0.083	17	97
880	1200	0.167	15	115
879	1200	0.25	24	154
895	1250	0.083	1177	1443
896	1250	0.167	1170	1410

I - volume attack (includes precipitation free zone)
II - total reaction zone.

Table 9: Reaction zone growth rate for the diffusion couple C/Hastelloy X as a function of temperature (900 - 1250°C)

Temperature °C	Reaction zone growth rate, x^2/t^*, cm^2/s	
	I	II
900	$3.76 \cdot 10^{-12}$	-
1000	$5{,}99 \cdot 10^{-11}$	-
1100	$4.71 \cdot 10^{-10}$	-
1200	$5.82 \cdot 10^{-9}$	$2.54 \cdot 10^{-7}$
1250	$2.9 \cdot 10^{-5}$	$4.28 \cdot 10^{-5}$

I - volume attack
II - total reaction zone

Table 10: Growth rate equations for the C/Hastelloy X interaction

Phenomena	Temperature range, °C	Growth rate equation, x^2/t, cm^2/s
Volume attack (I)	900 - 1200	$9.2 \cdot 10^3 \exp(-346208/RT)$
Volume attack (I)	1200 - 1250	*
Total reaction zone (II)	1200 - 1250	$1.32 \cdot 10^{62} \exp(-1937525/RT)$

*: no calculation possible $\rightarrow$pre exponential factor $\rightarrow \infty$
R= 8.314 J/mol K

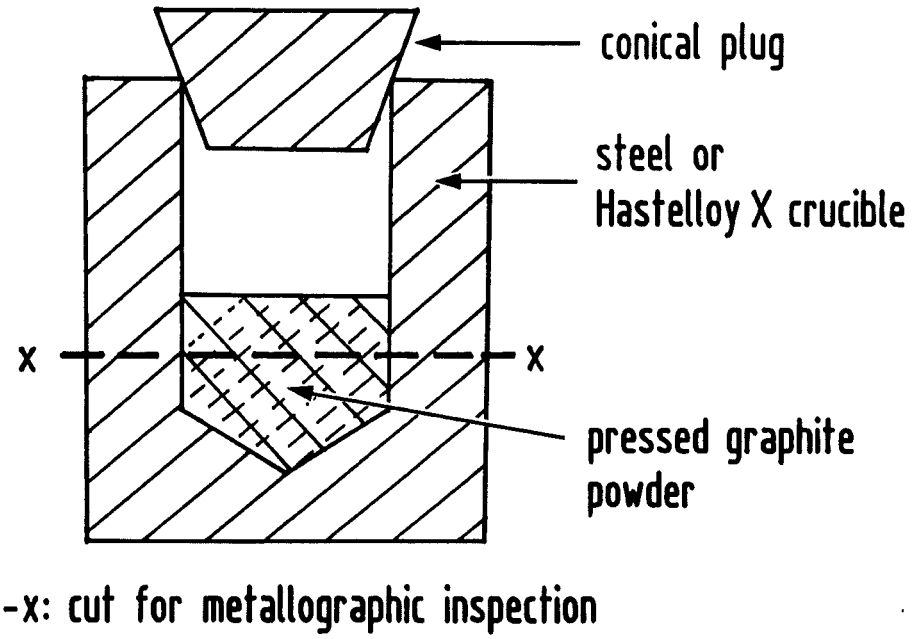

Fig. 1: Schematic of the annealing capsules used in the compatibility experiments.

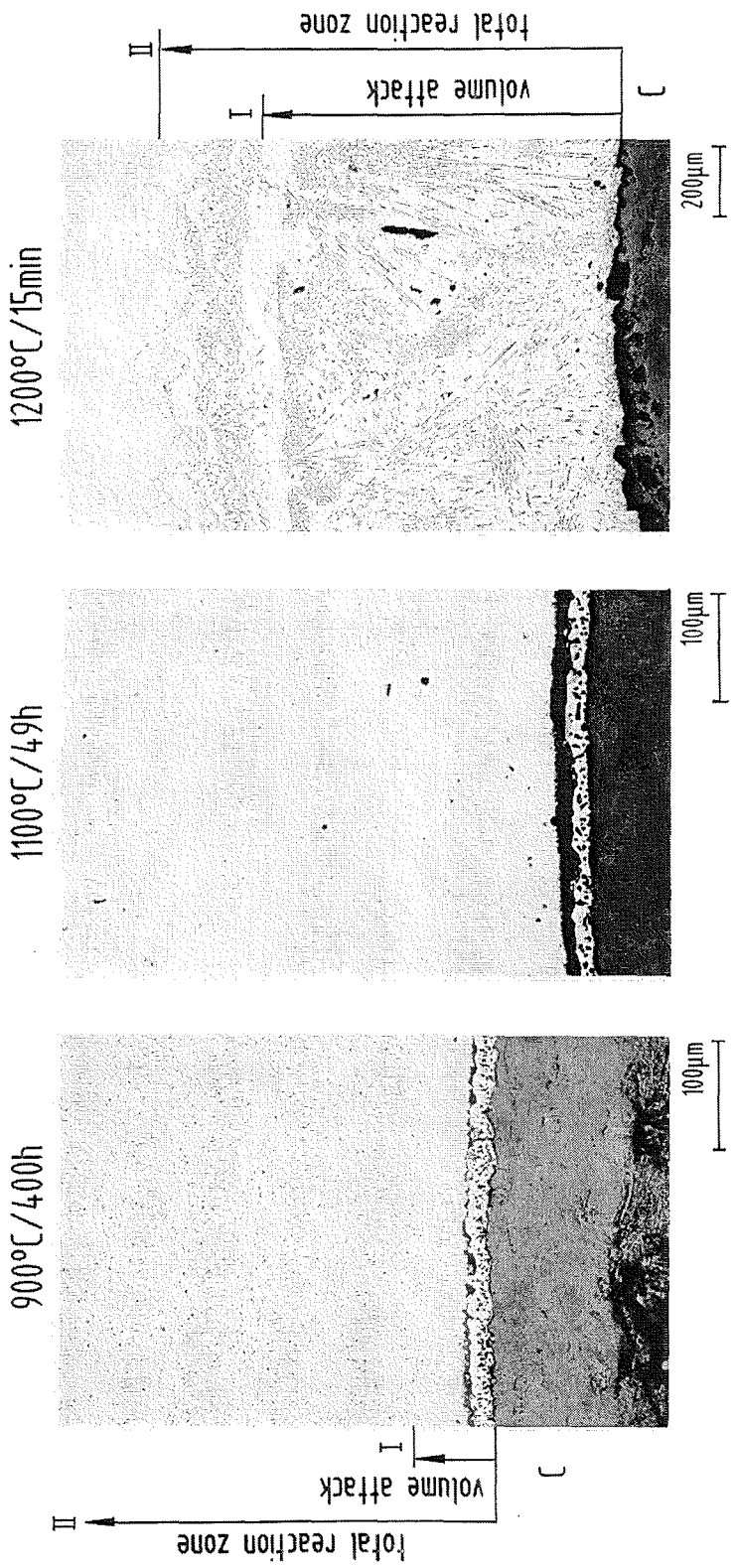

Fig. 2: Chemical interactions between C (graphite) and 1.4914 ferritic steel for different temperature-time combinations.

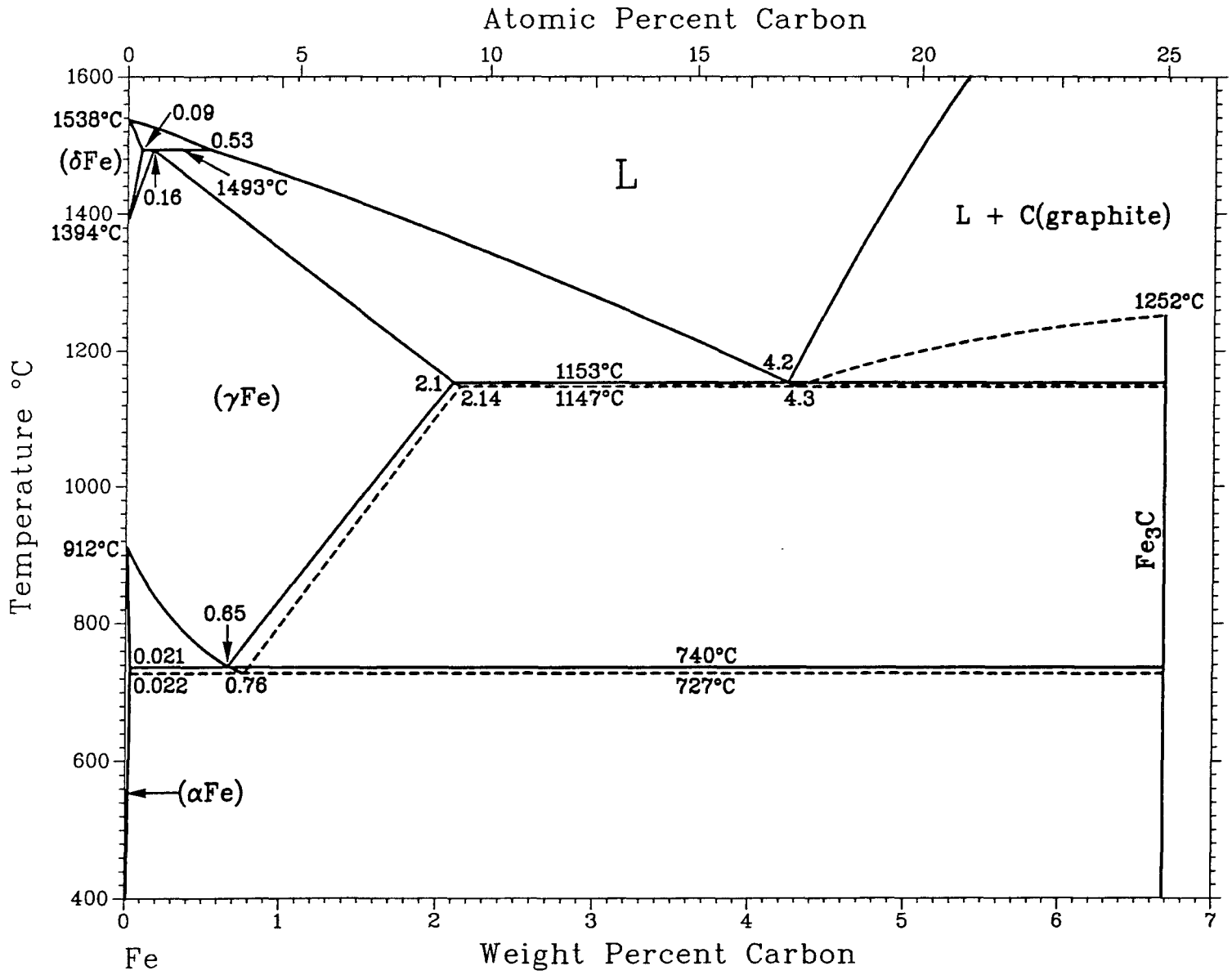

Fig. 3: Binary alloy phase diagram of the Fe-C system [1].

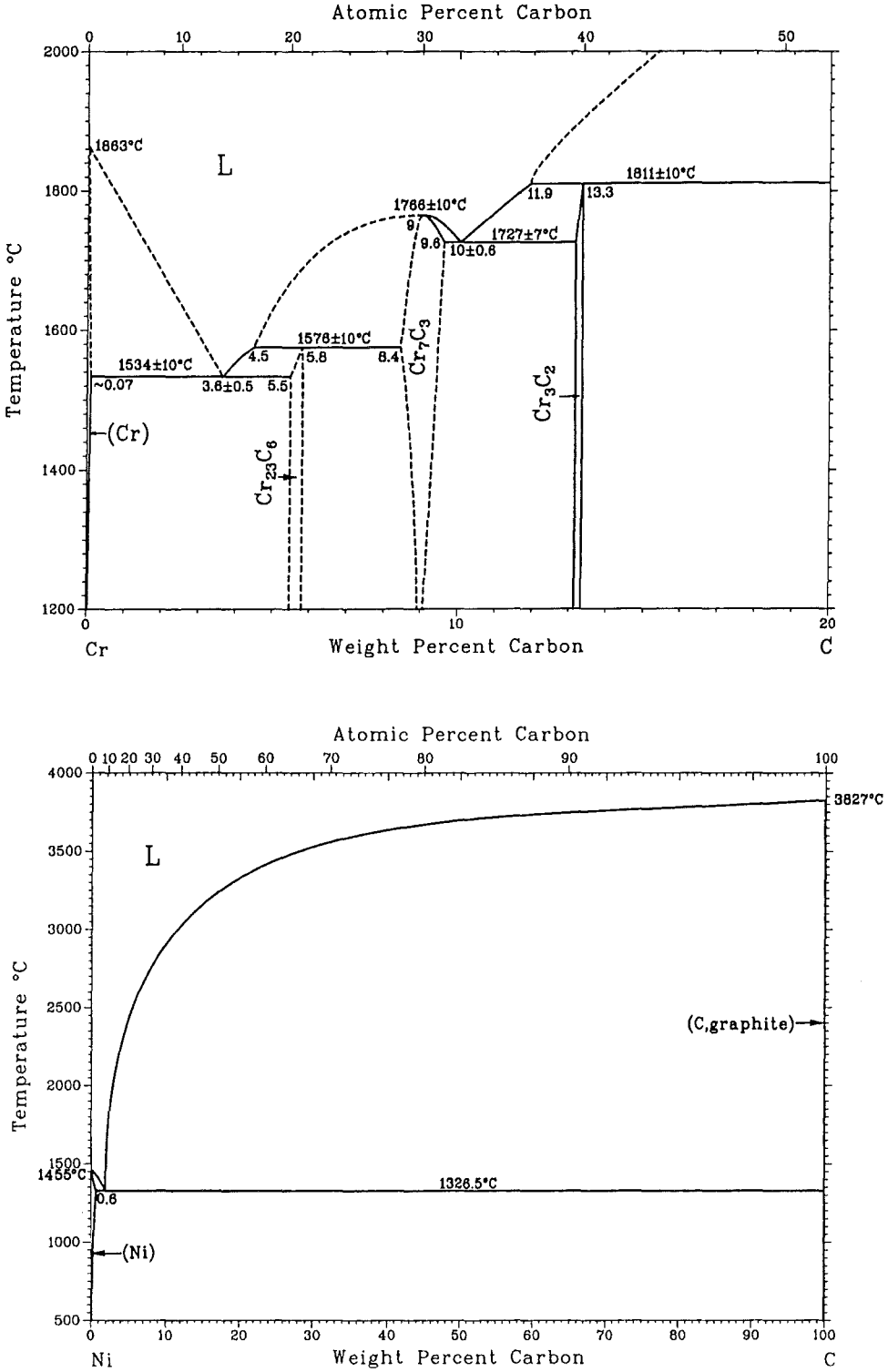

Fig. 4: Binary alloy phase diagrams of the Cr-C and Ni-C systems, respectively [1, 2].

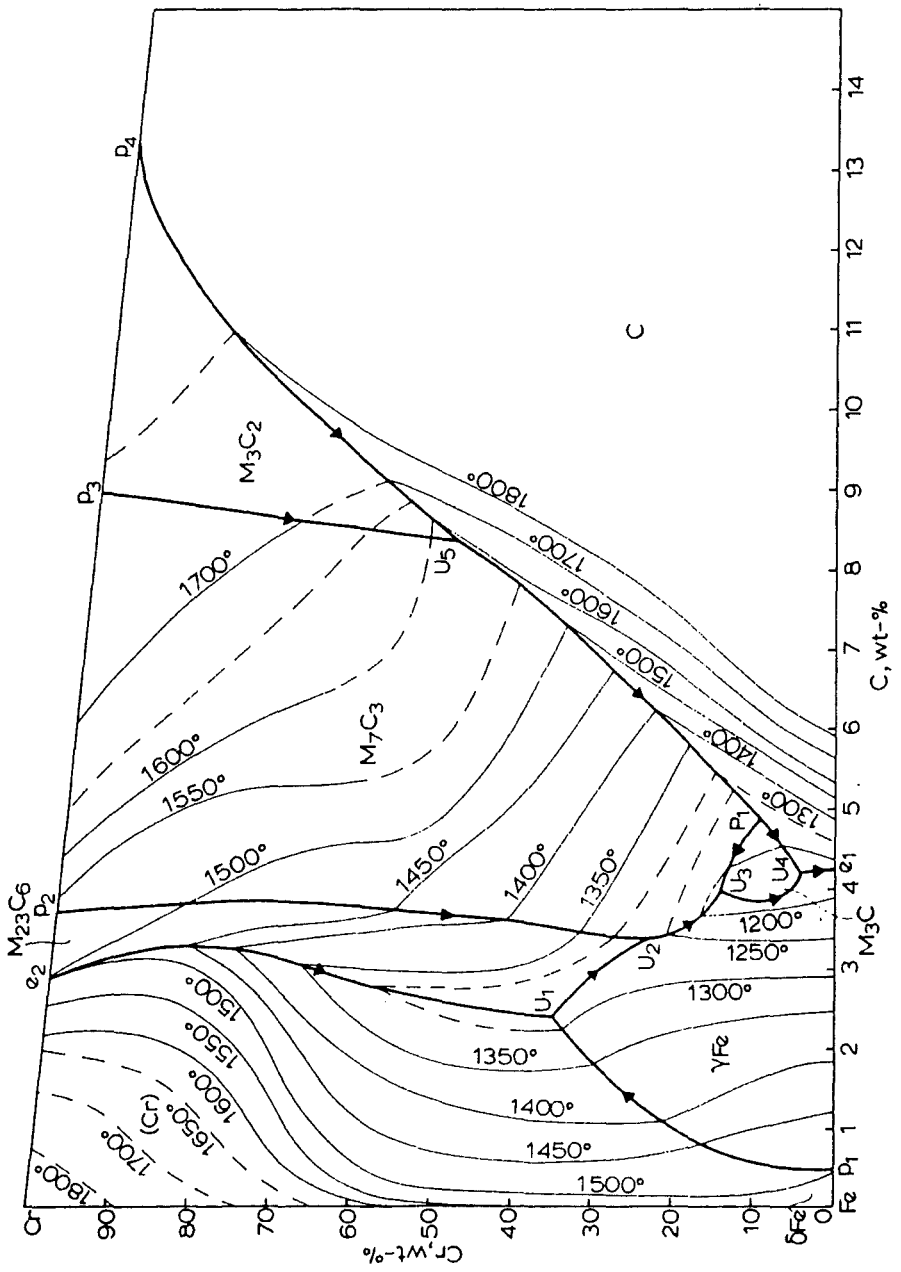

Fig. 5: Liquidus projection diagram of the C-Cr-Fe system [3].

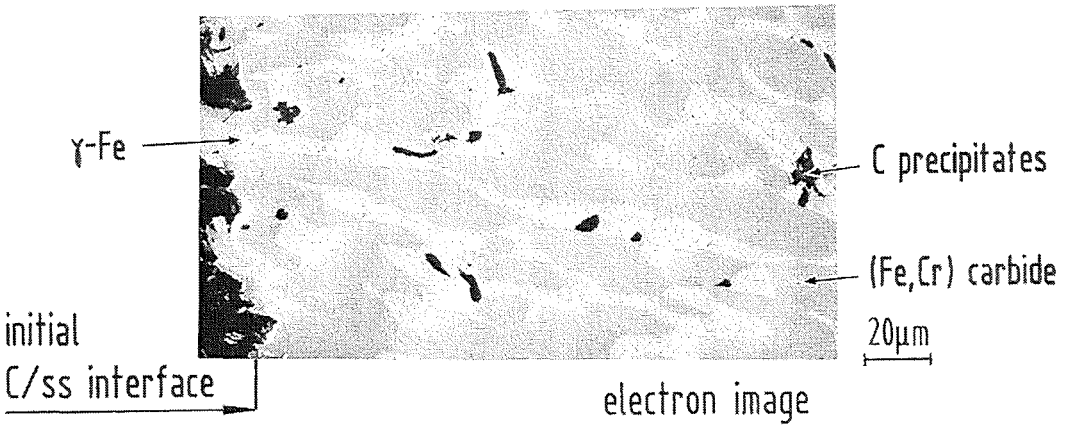

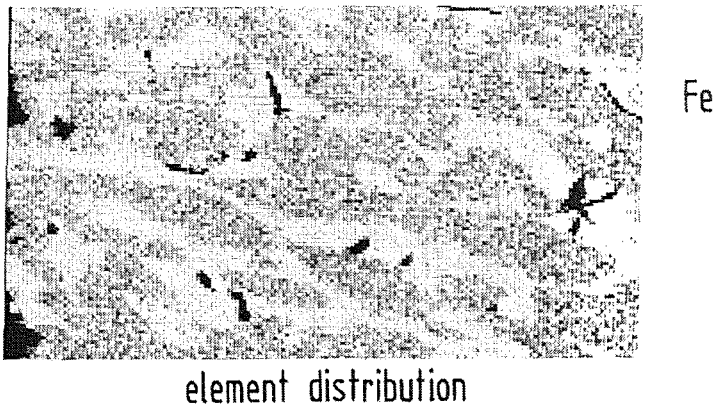

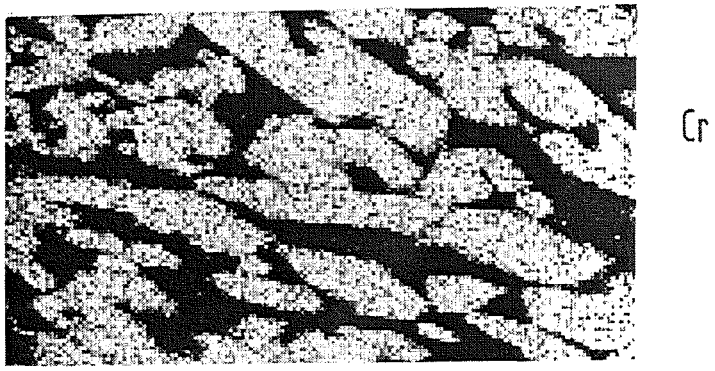

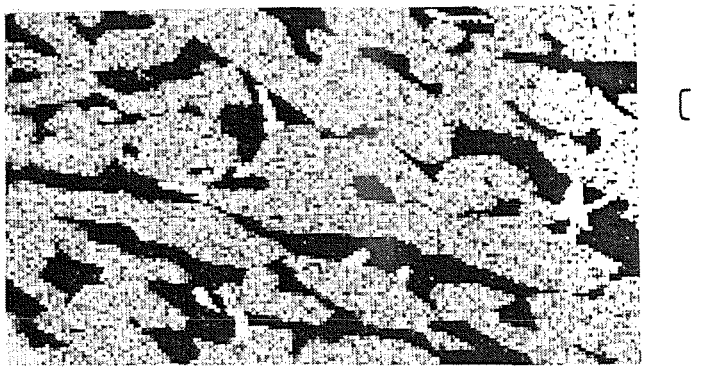

Fig. 6: Chemical composition of the reaction layer I for the graphite/1.4914 ferritic steel system after 5 min at 1250°C.

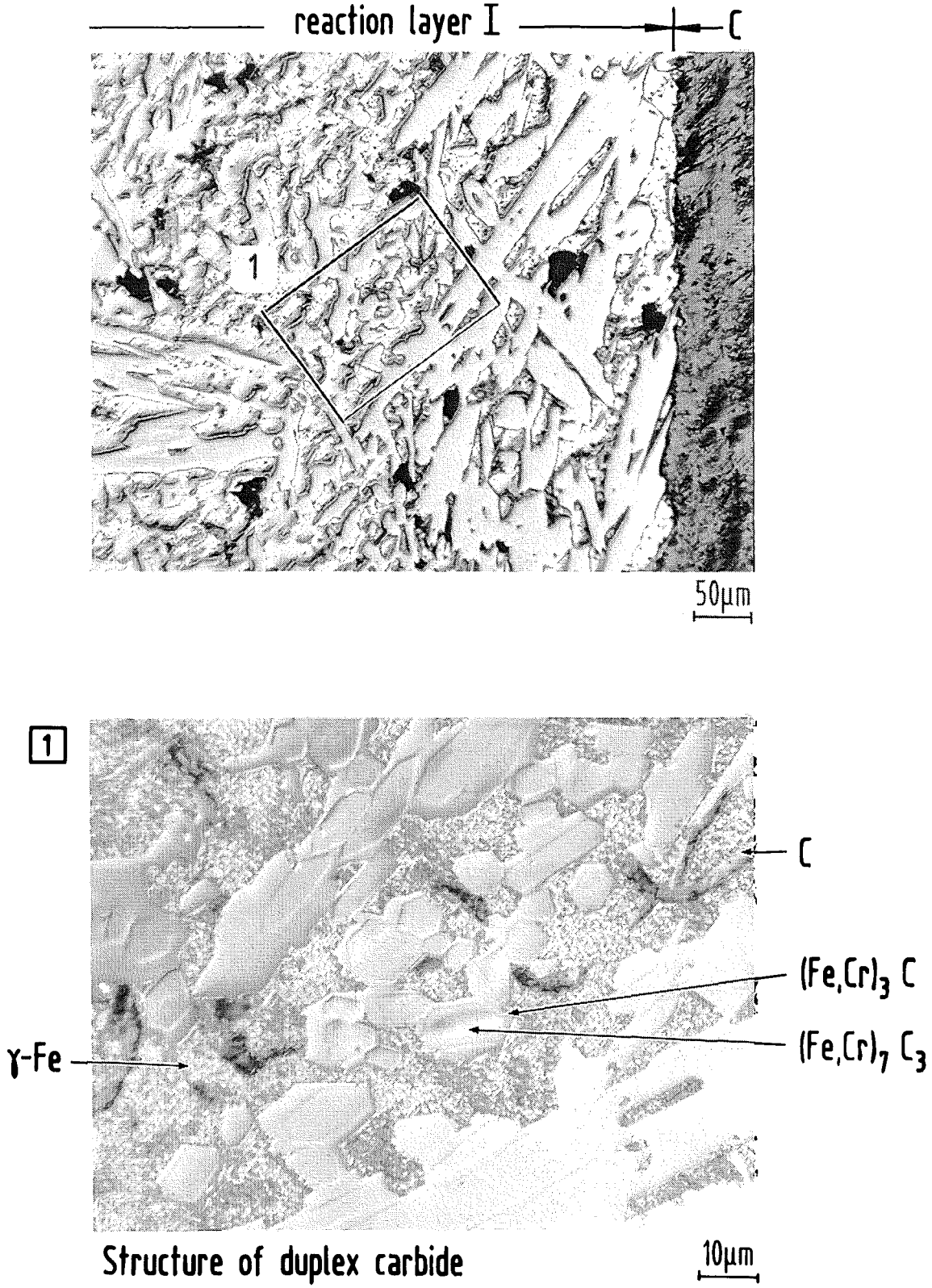

Fig. 7: Chemical interactions between graphite and 1.4914 ferritic steel ater 5 min at 1250°C; formation of a duplex carbide.

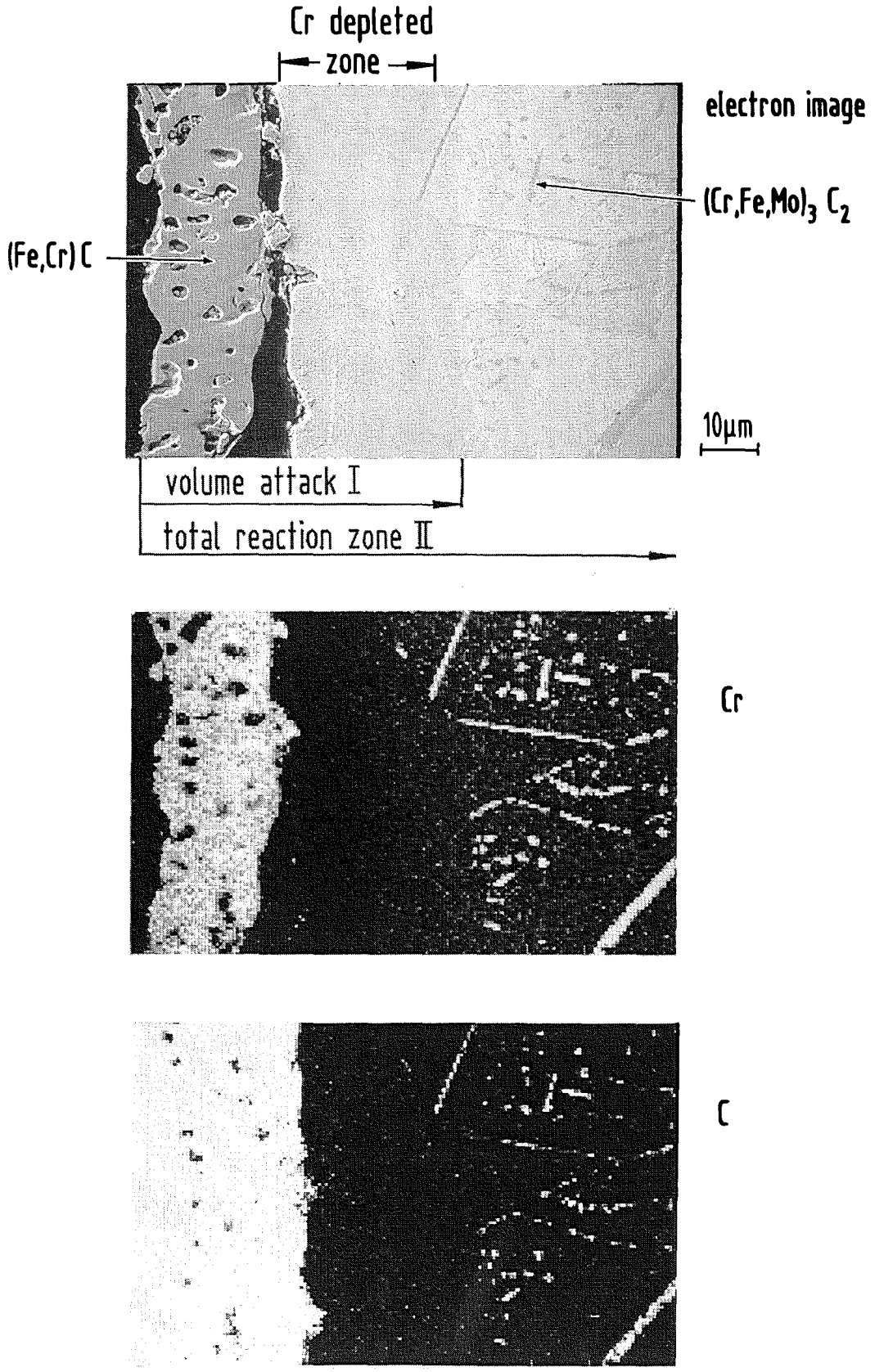

Fig. 8: Chemical composition of the graphite/1.4914 ferritic steel reaction zone after 100 h at 1100°C.

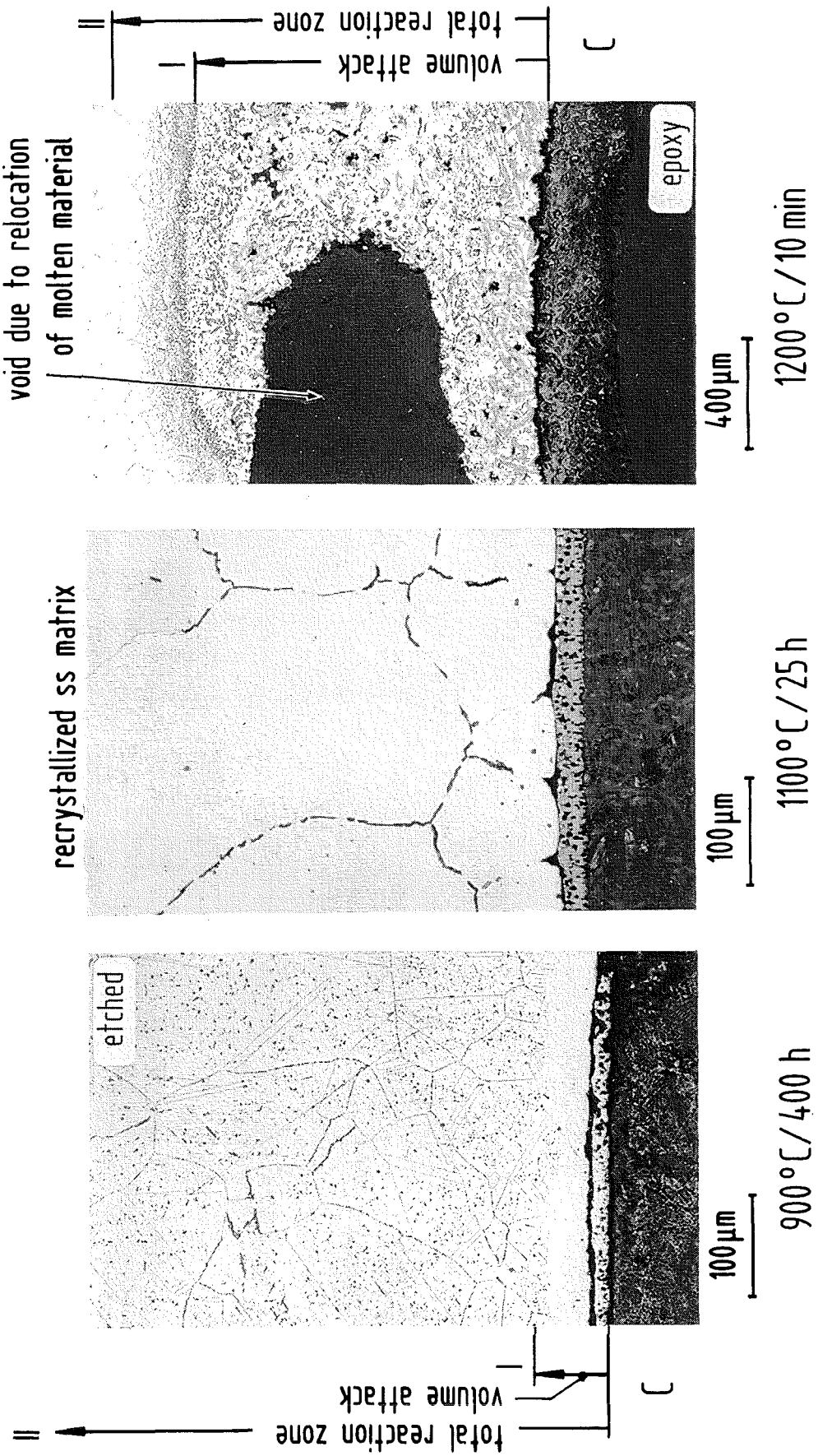

Fig. 9: Chemical interactions between graphite and 1.4919 stainless steel for different temperature-time combinations.

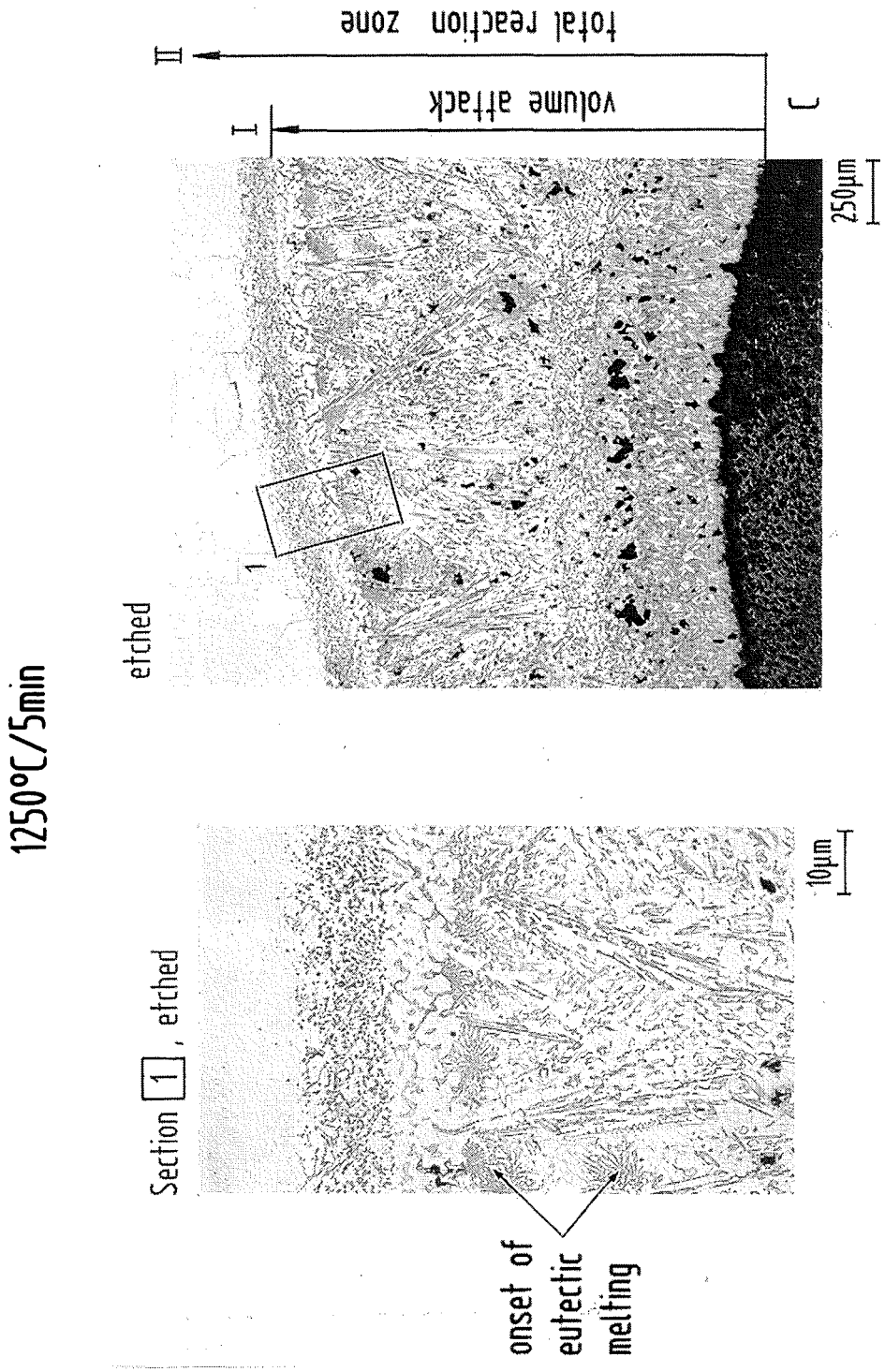

Fig. 10: Chemical interactions between graphite and 1.4919 stainless steel after 5 min at 1250°C.

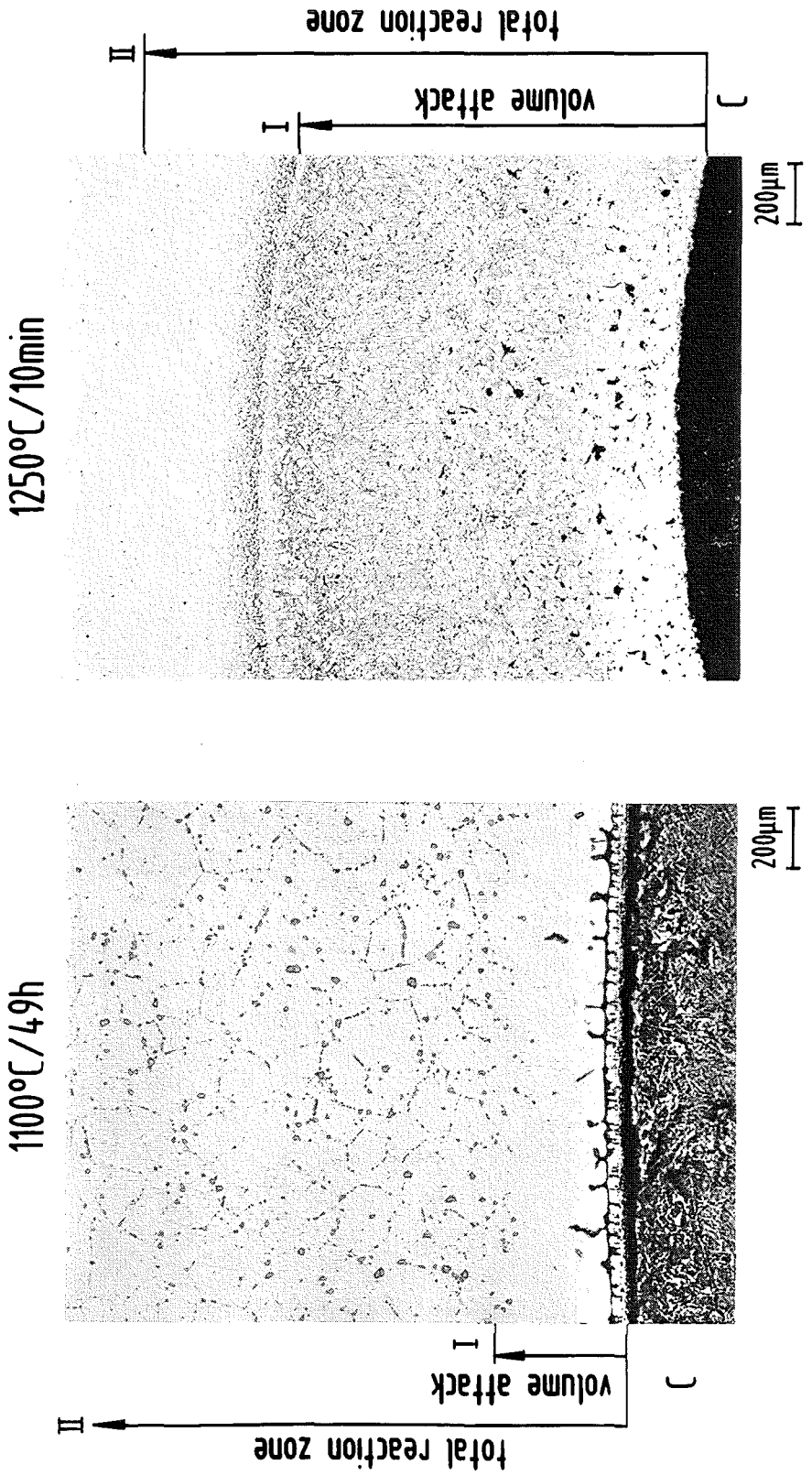

Fig. 11: Chemical interactions between graphite and Hastelloy X at 1100 and 1250°C.

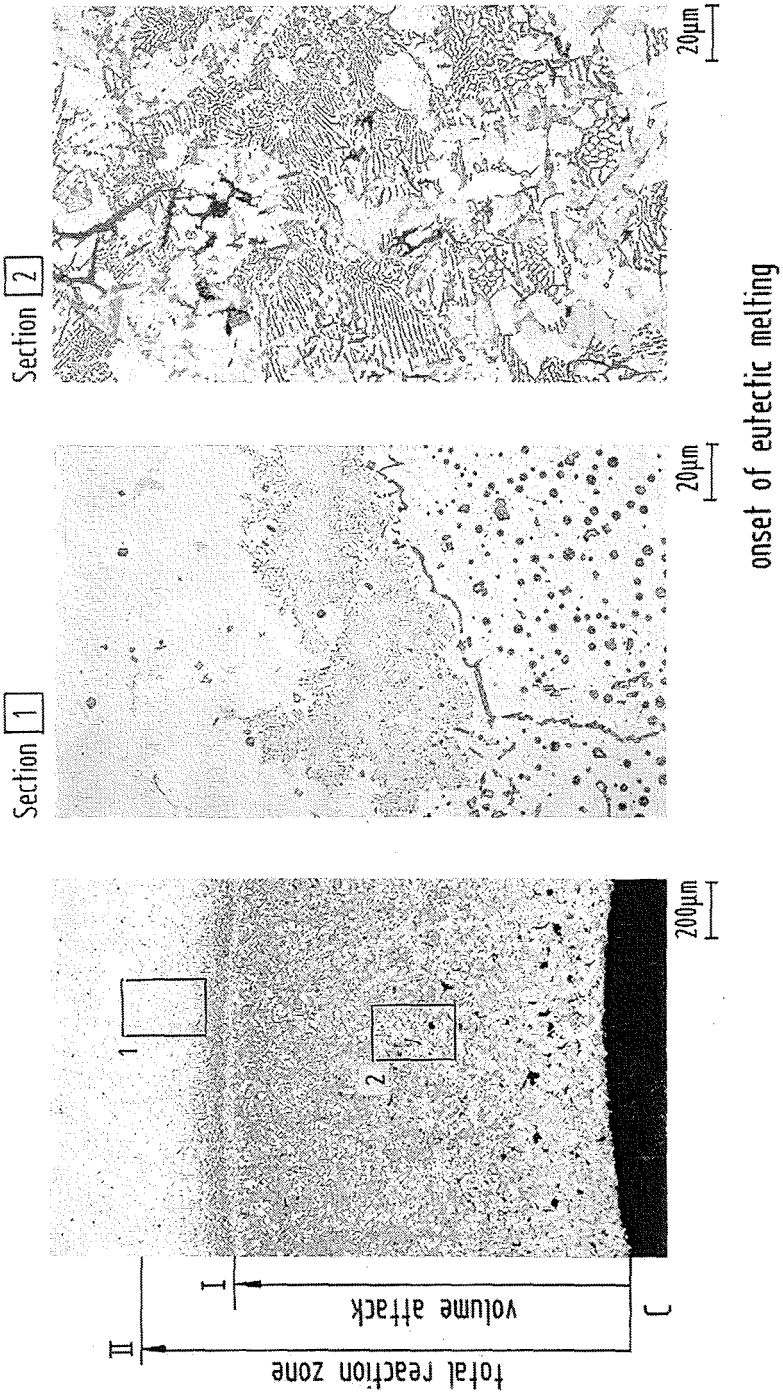

Fig. 12: Chemical interactions between graphite and Hastelloy X after 10 min at 1250°C.

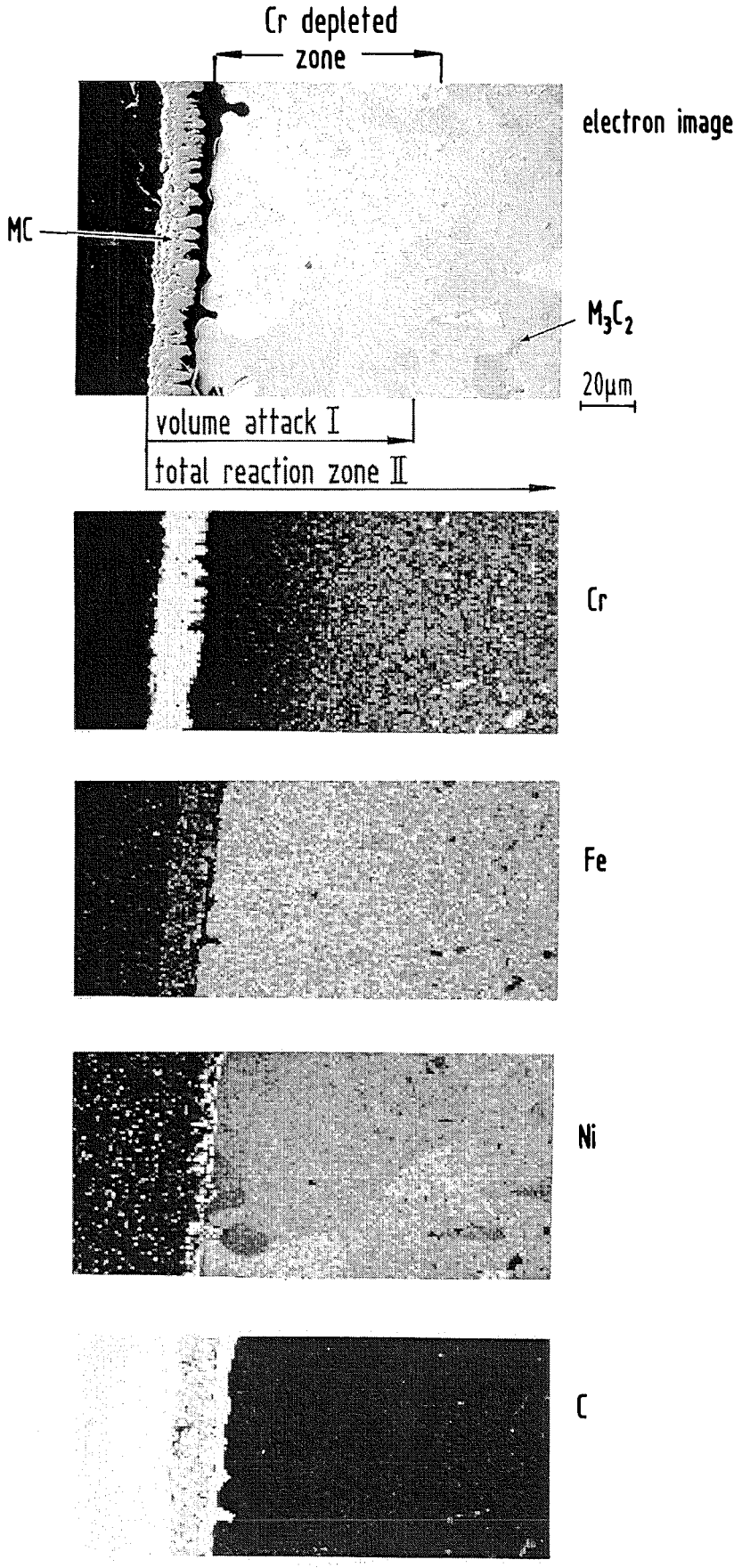

Fig. 13: Chemical composition of the graphite/Hastelloy X reaction zone after 49 h at 1100°C.

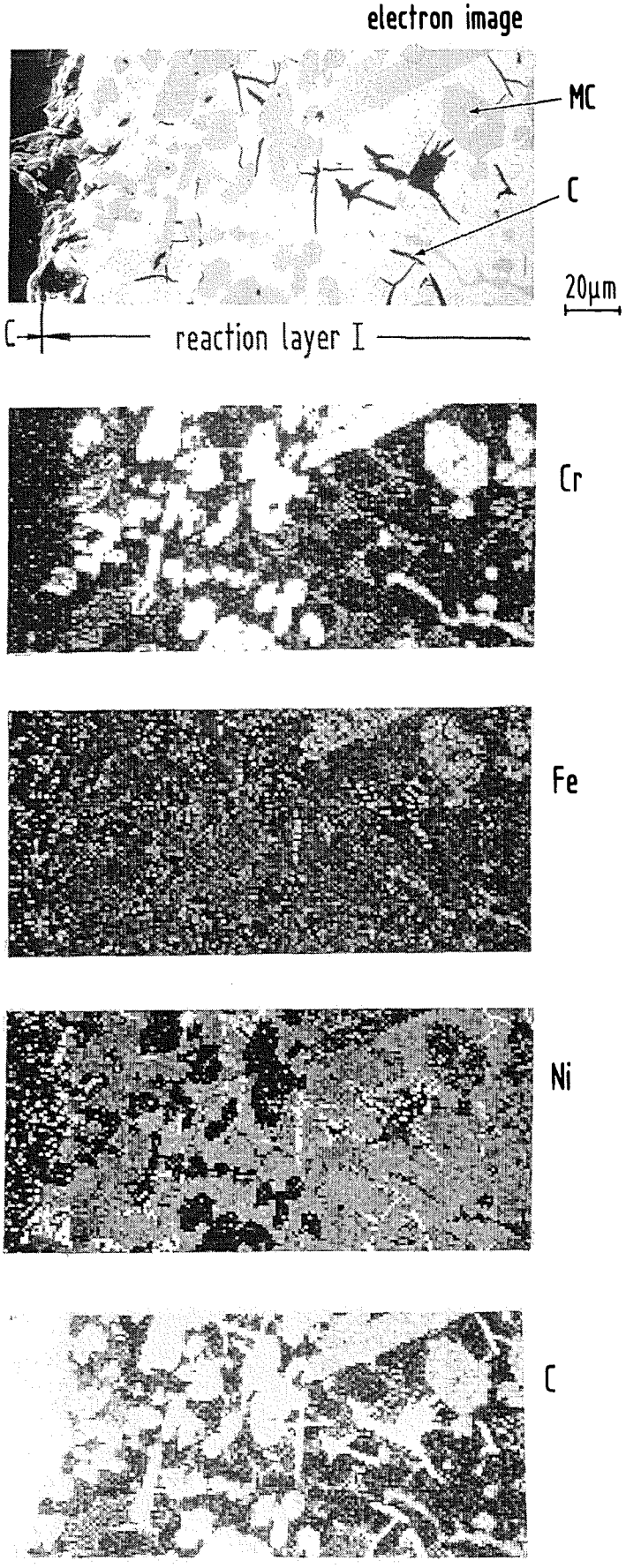

Fig. 14: Chemical composition of the reaction layer I for the graphite/Hastelloy X system after 15 min at 1250°C.

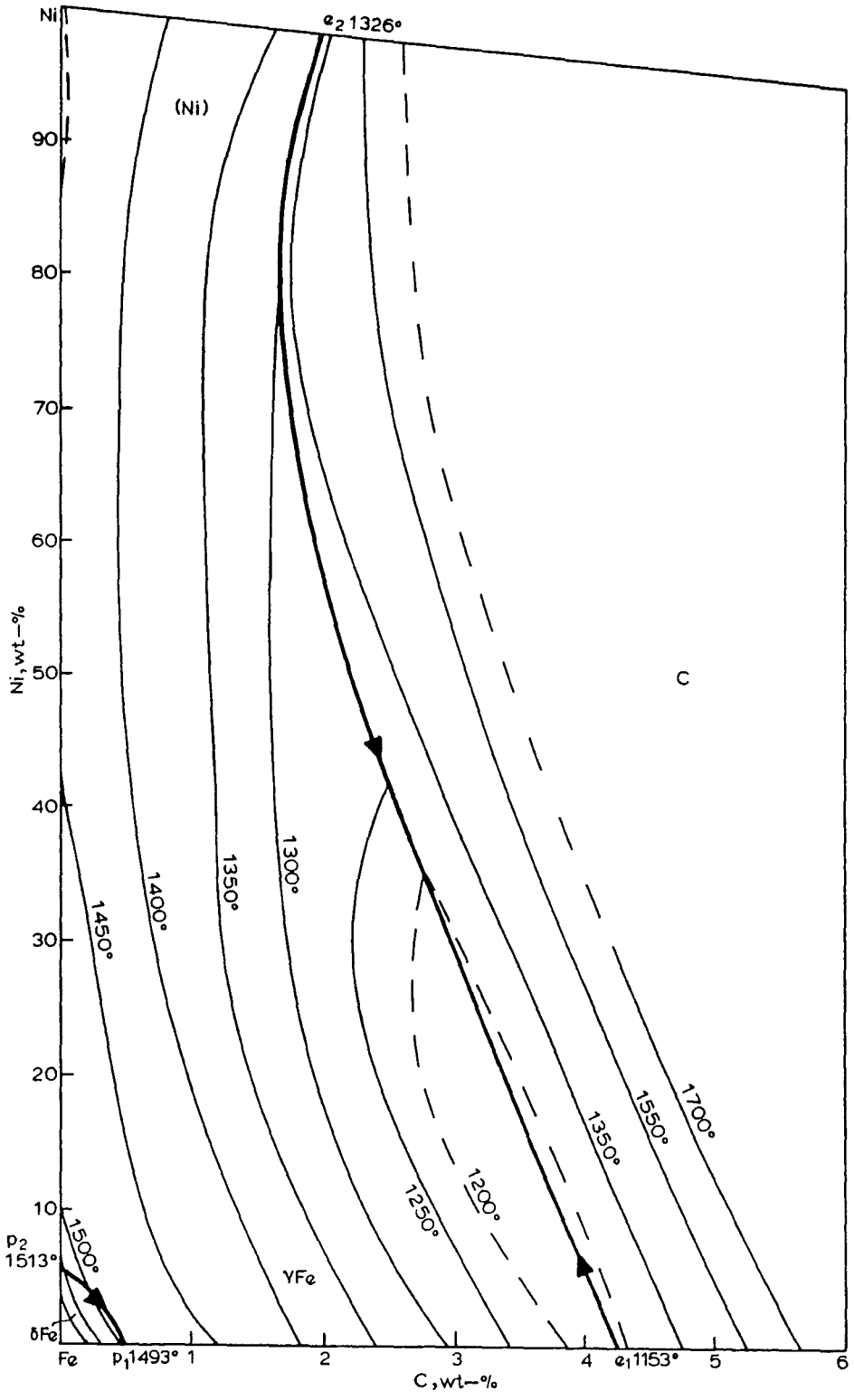

Fig. 15: Liquidus projection diagram for the C-Fe-Ni system [9].

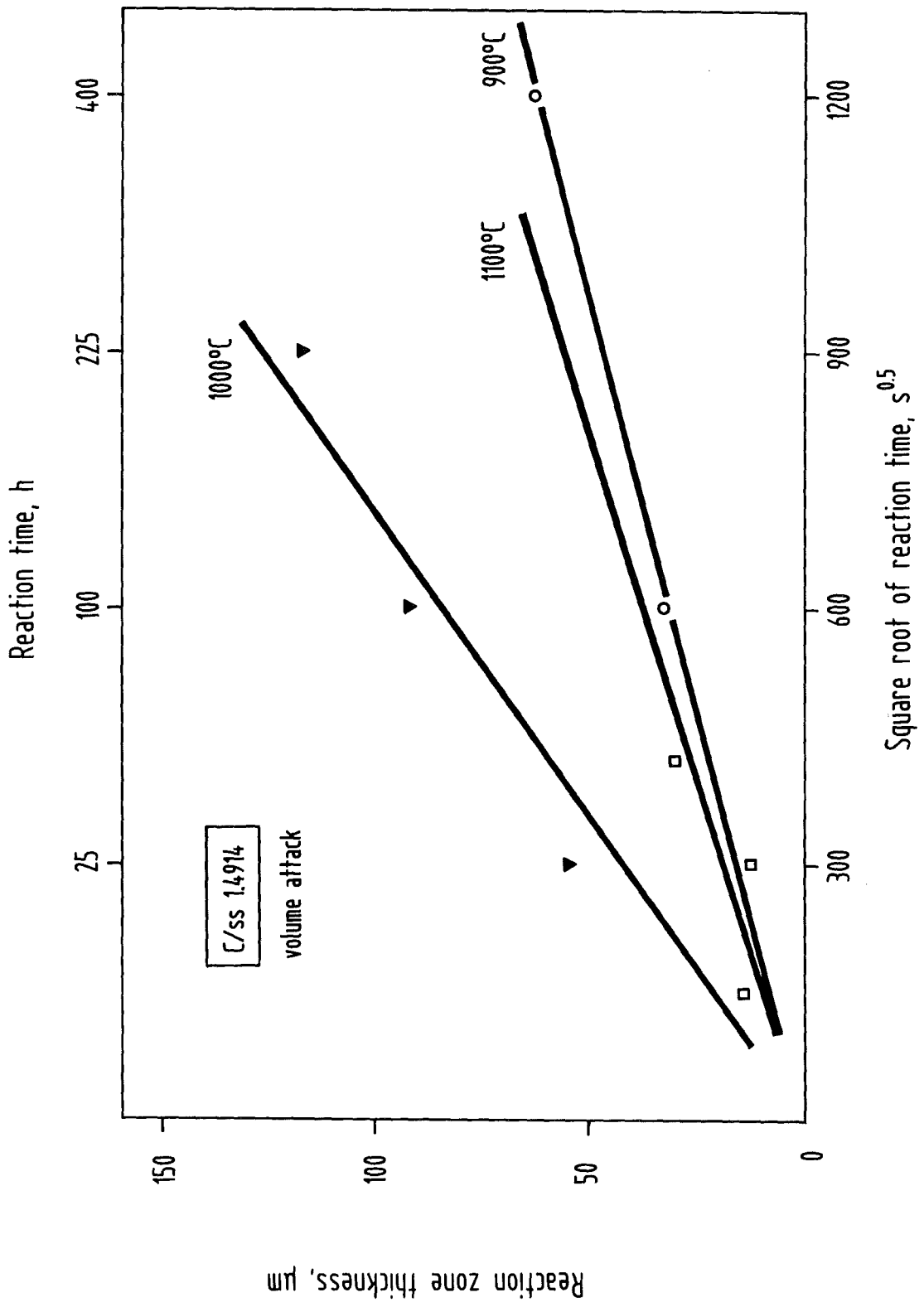

Fig. 16: Maximum volume attack thicknesses in 1.4914 ferritic steel versus square root of time between 900 and 1100°C (Table 2).

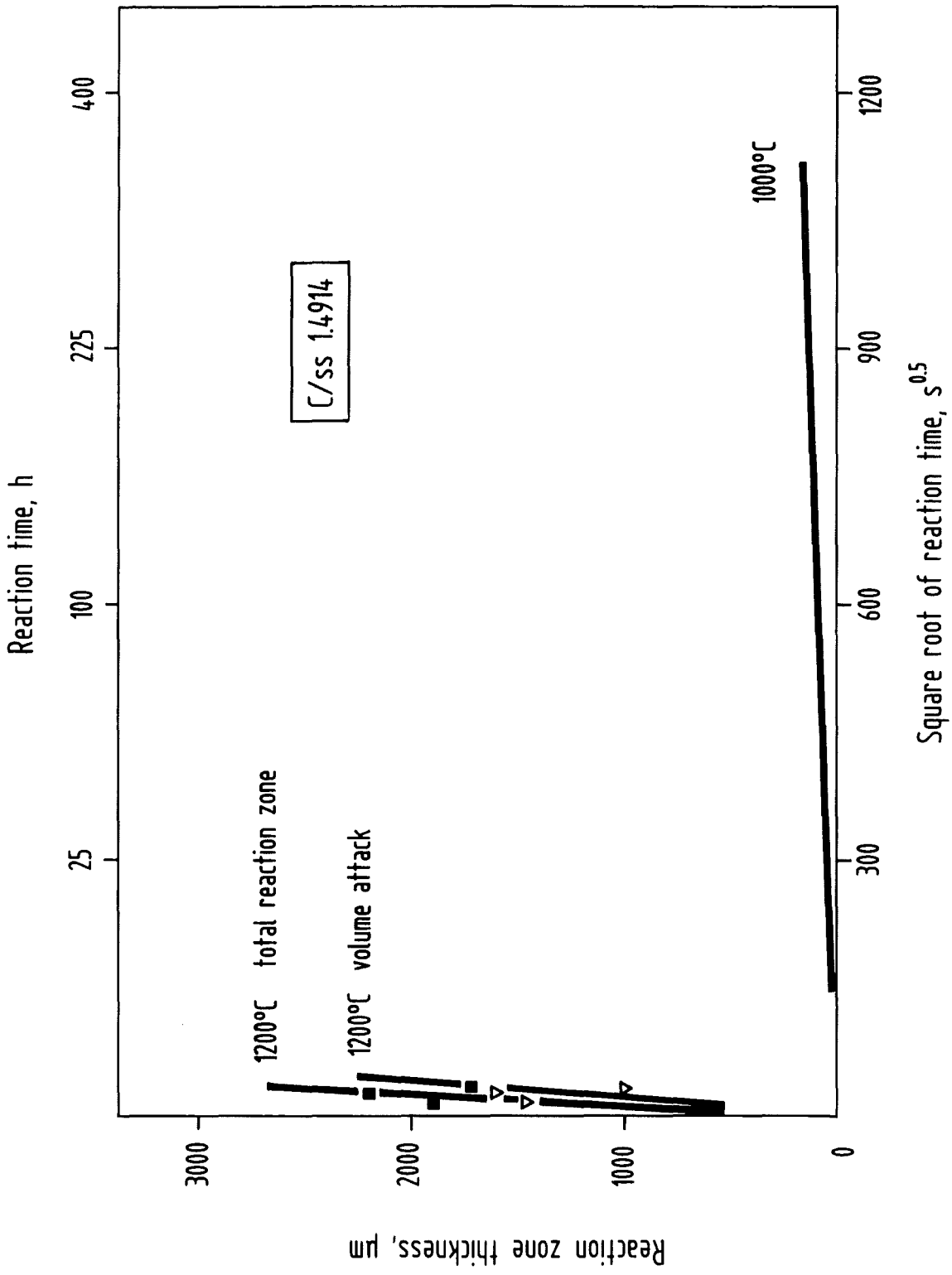

Fig. 17: Maximum volume attack and total reaction zone thicknesses in 1.4914 ferritic steel versus square root of time at 1200°C (Table 2).

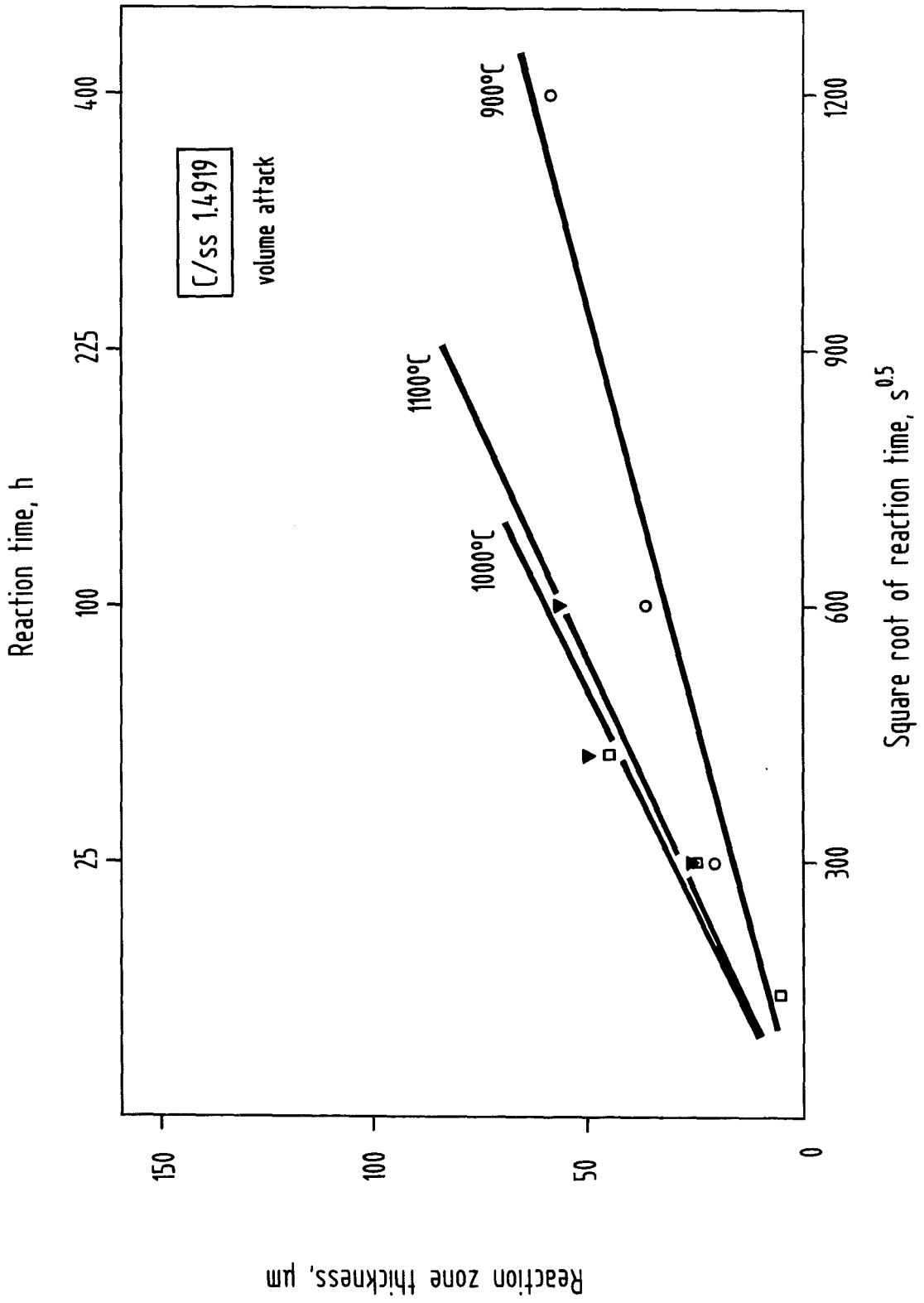

Fig. 18: Maximum volume attack thicknesses in 1.4919 stainless steel versus square root of time between 900 and 1100°C (Table 5).

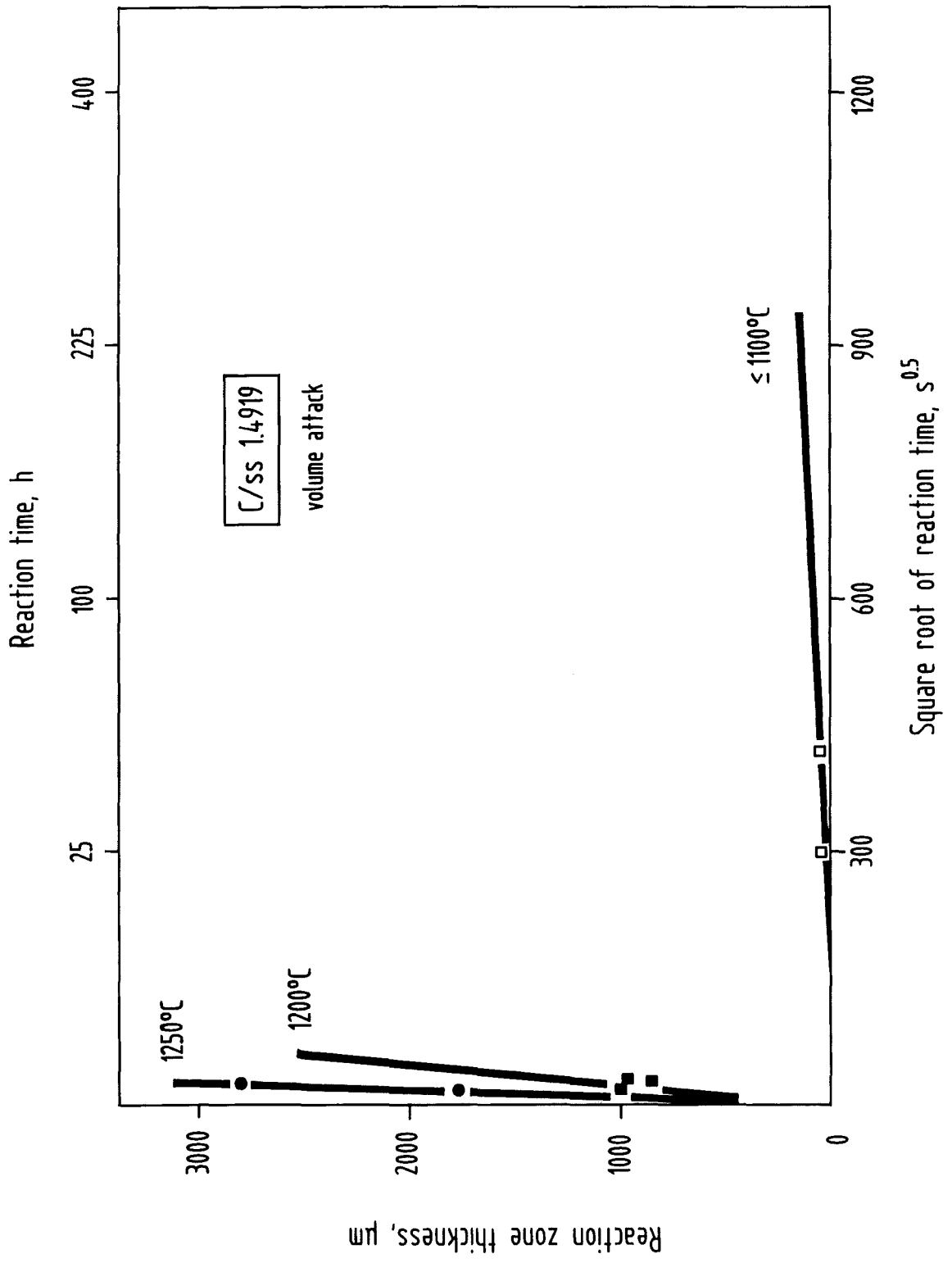

Fig. 19: Maximum volume attack thicknesses in 1.4919 stainless steel versus square root of time at 1200 and 1250°C (Table 5).

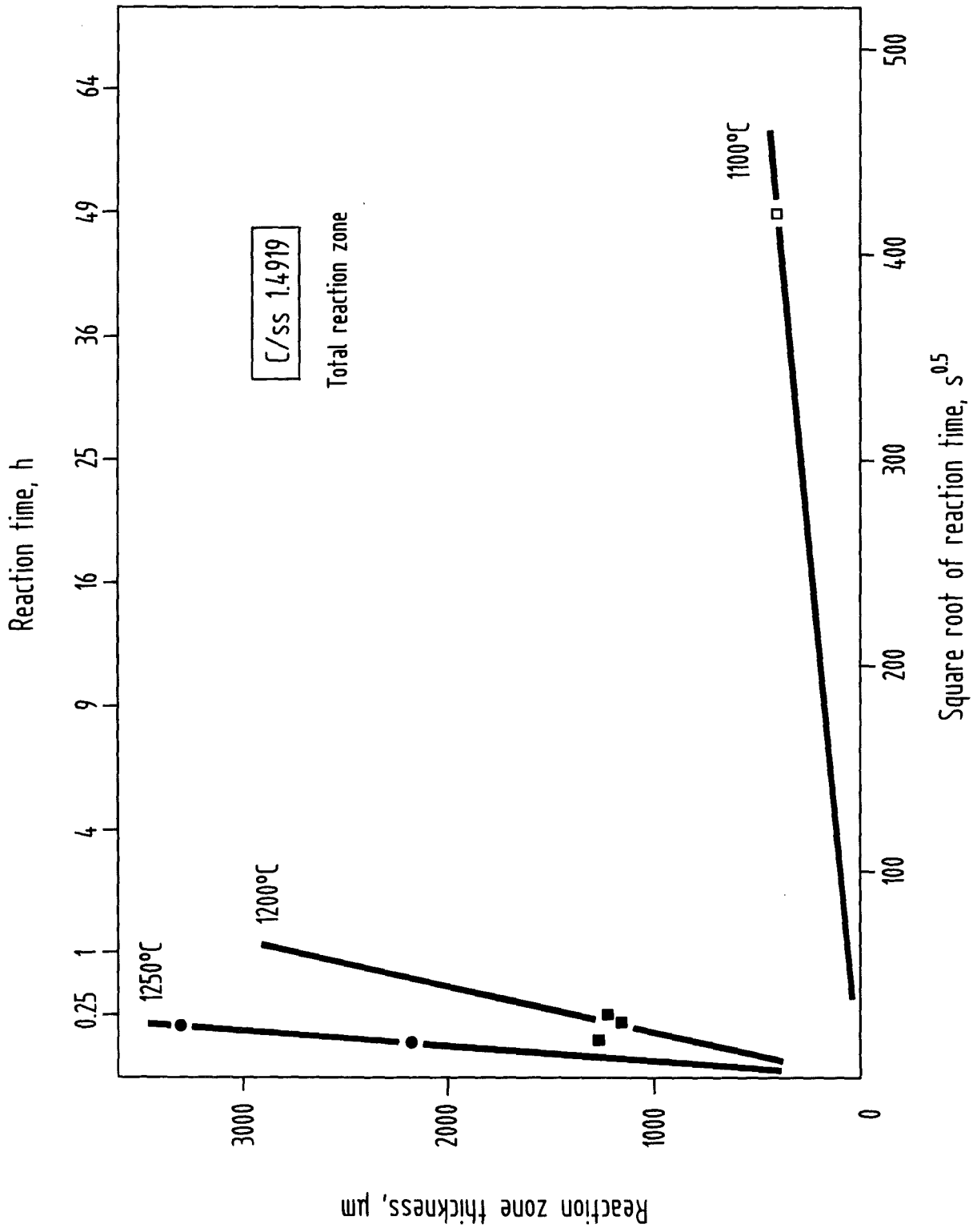

Fig. 20: Total reaction zone thicknesses in 1.4919 stainless steel versus square root of time between 1100 and 1250°C (Table 5).

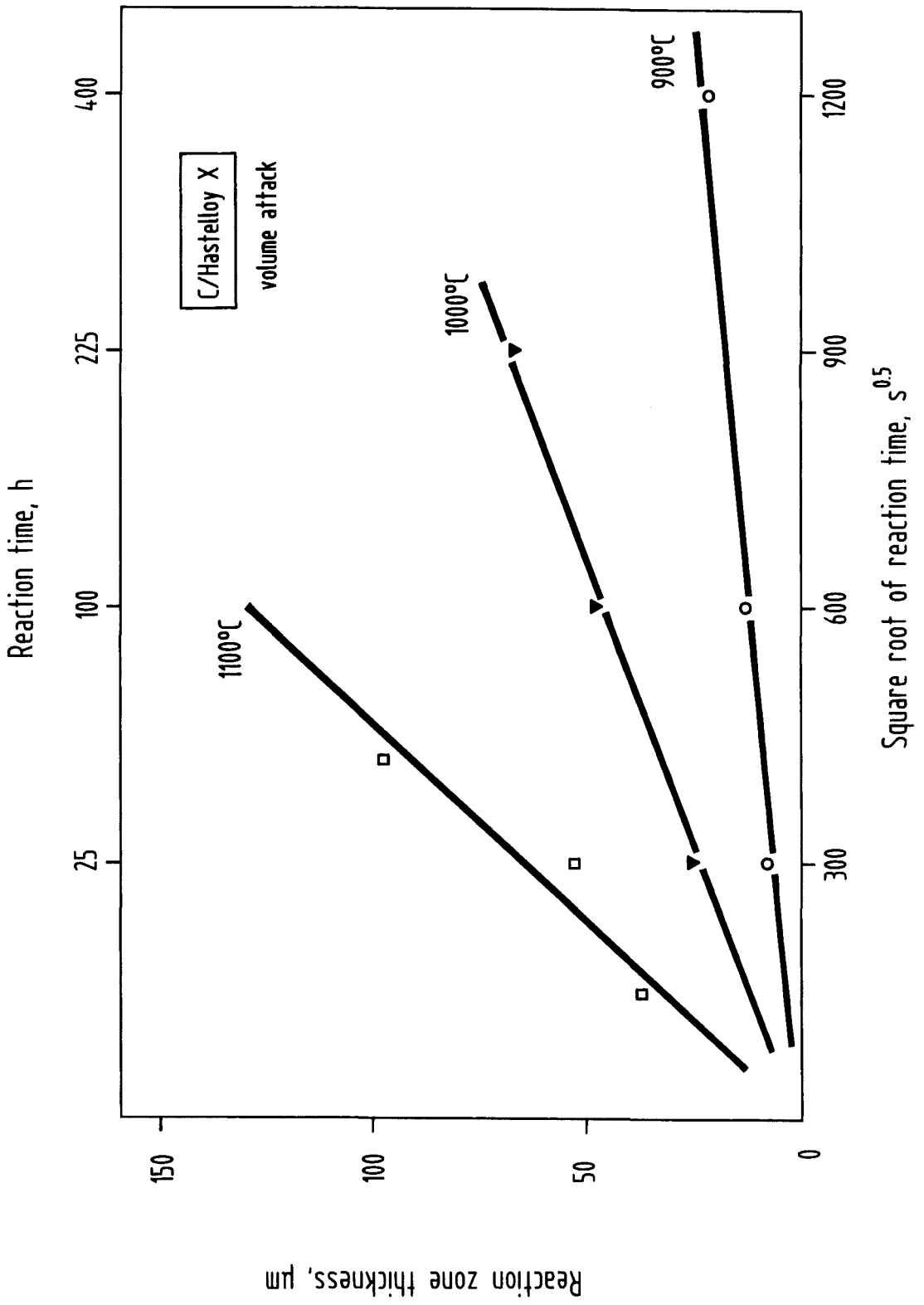

Fig. 21: Maximum volume attack thicknesses in Hastelloy X versus square root of time between 900 and 1100 °C (Table 8).

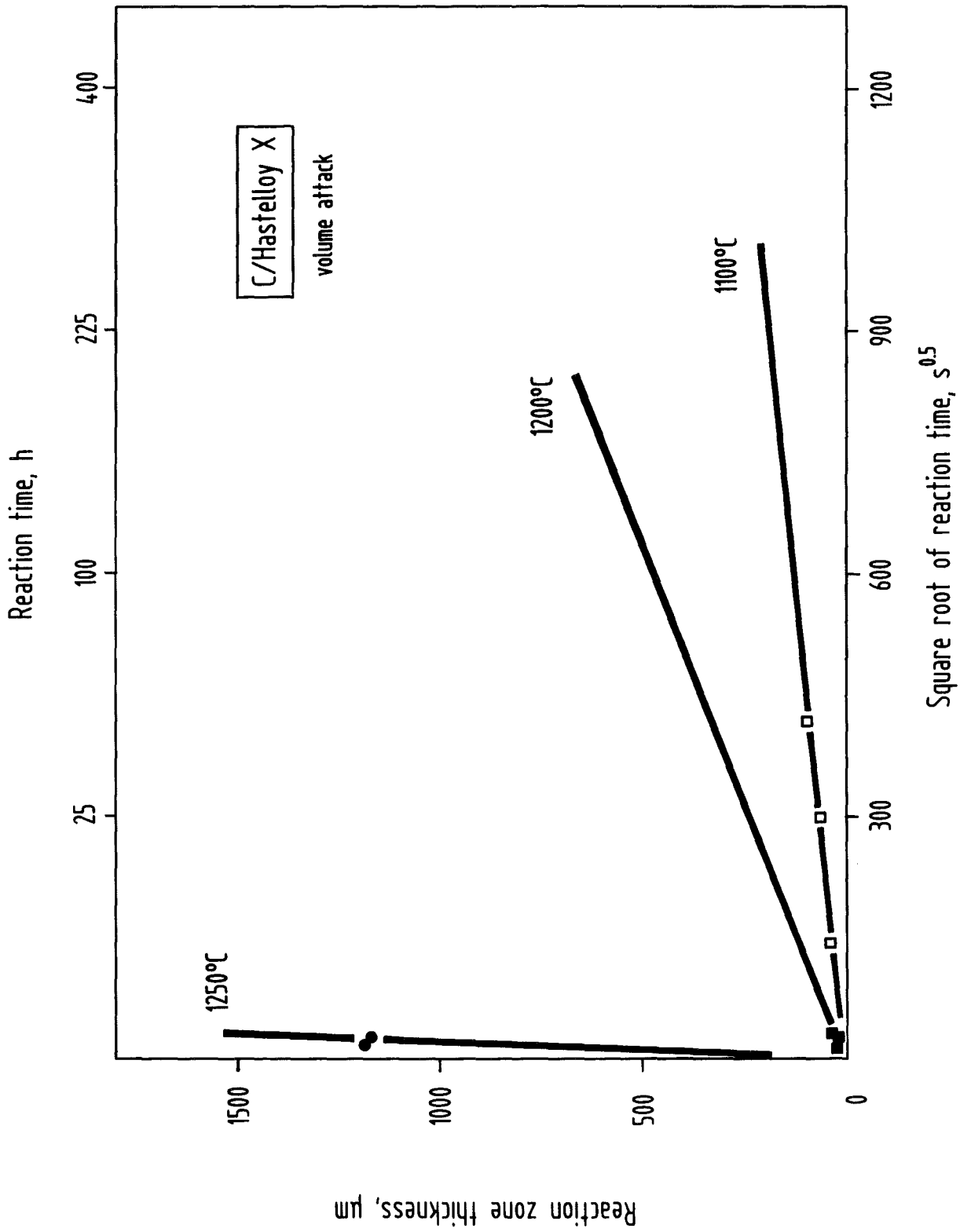

Fig. 22: Maximum volume attack thicknesses in Hastelloy X versus square root of time between 1100 and 1250°C (Table 8).

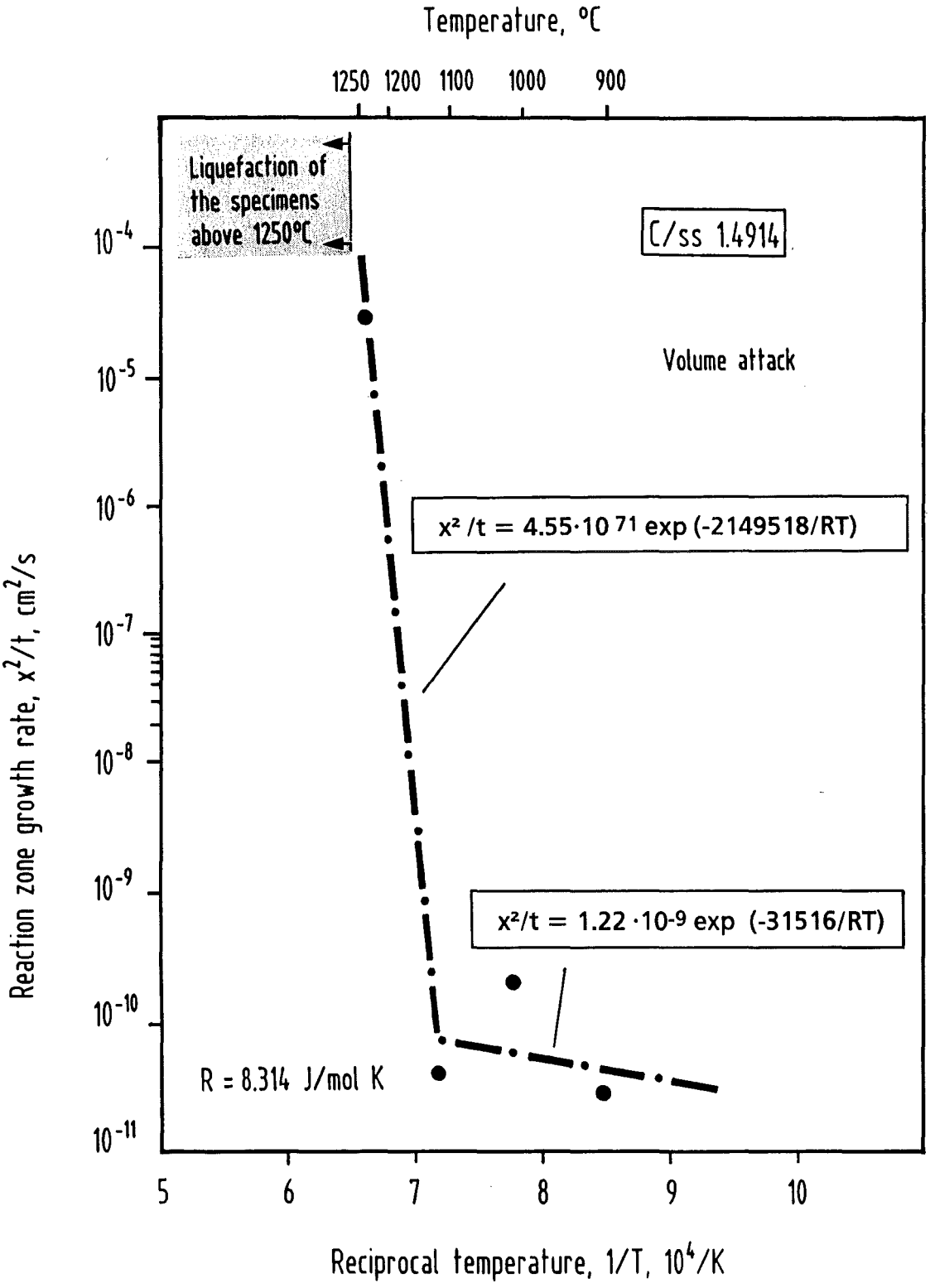

Fig. 23: Reaction zone growth rate in 1.4914 stainless steel for the graphite 1.4914 ferritic steel system (Table 3).

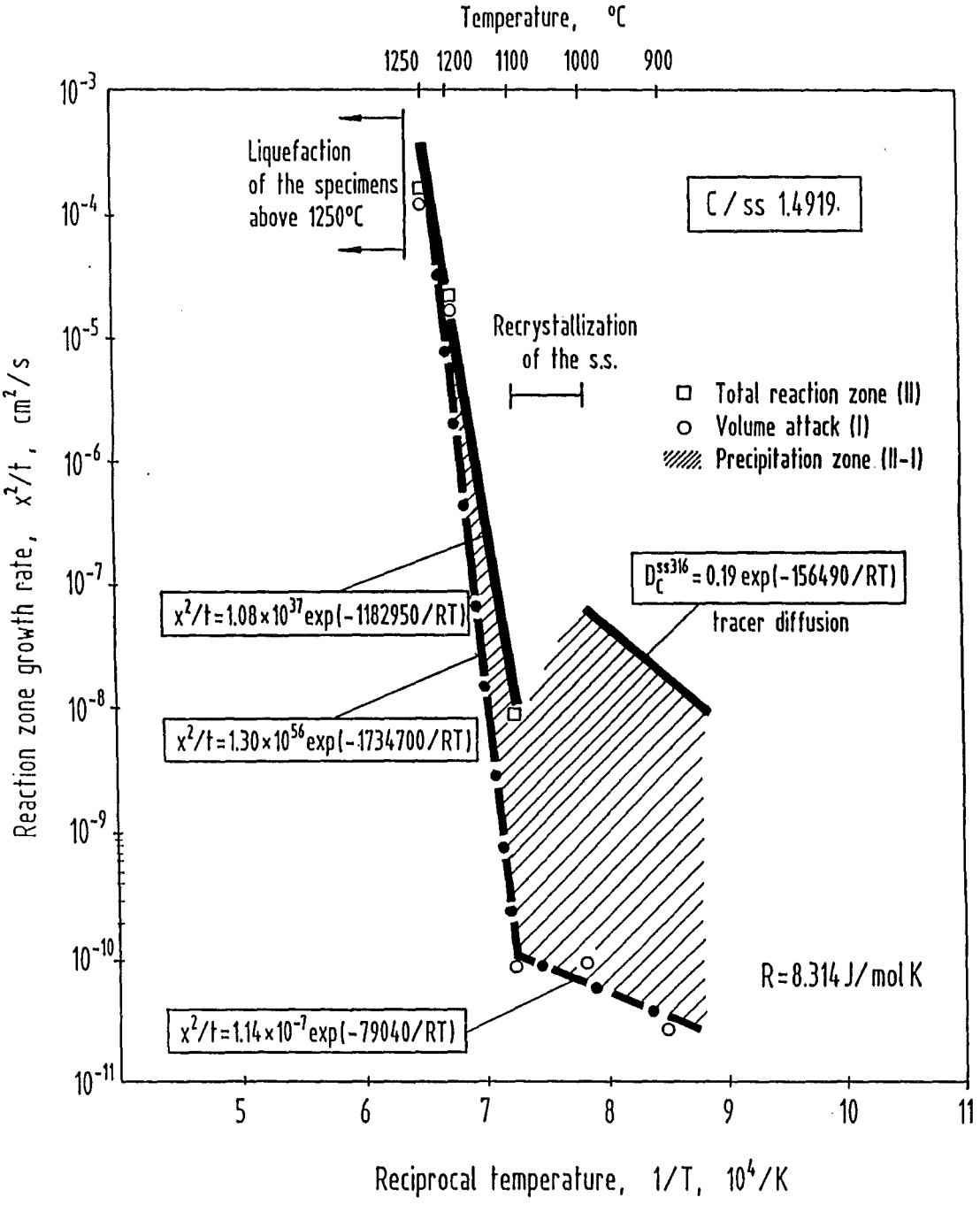

Fig. 24: Reaction zone growth rate in 1.4919 stainless steel for the graphite/1.4919 stainless steel system (Table 6).

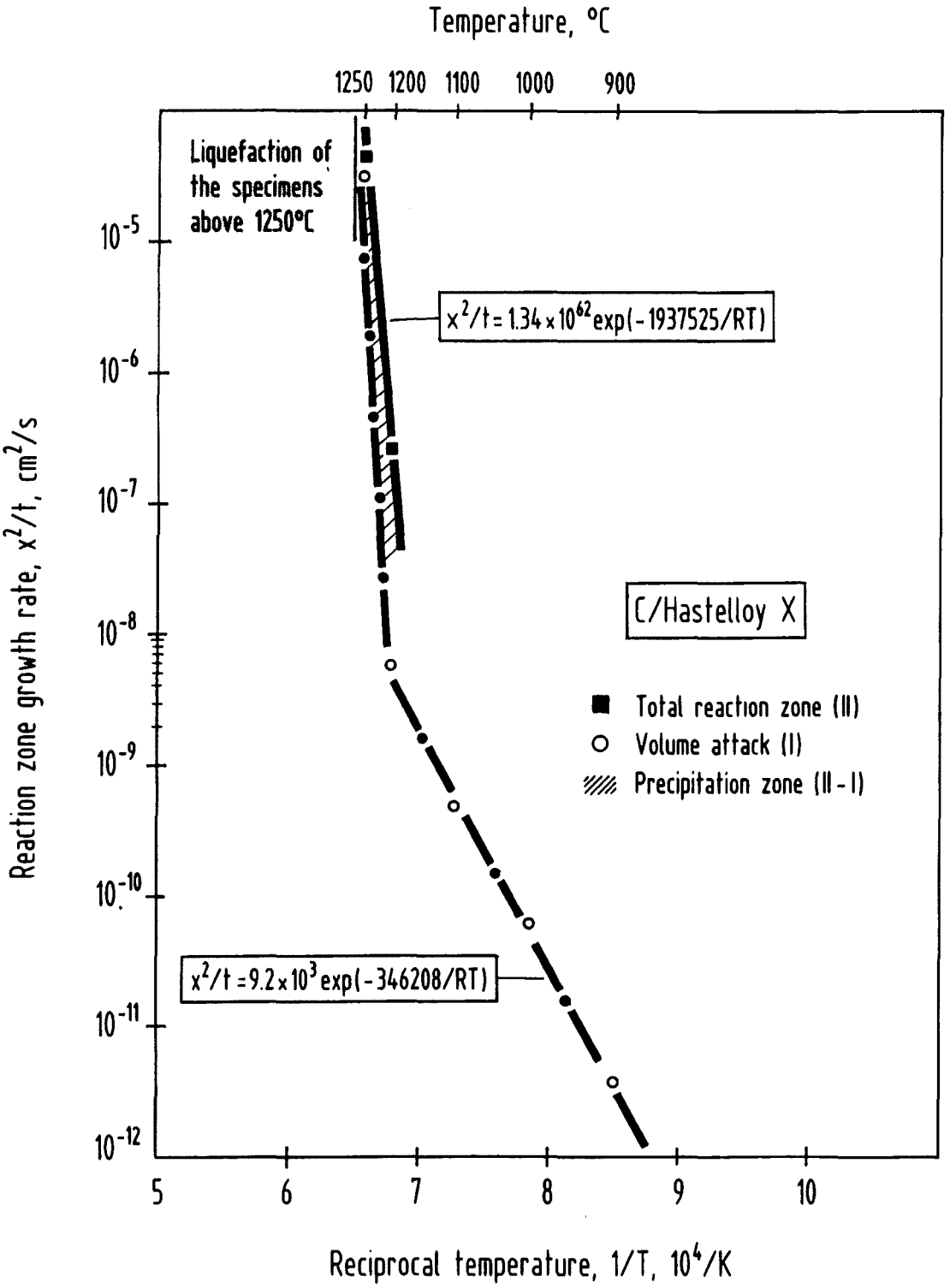

Fig. 25: Reaction zone growth rate in Hastelloy X for the graphite/Hastelloy X system (Table 9).

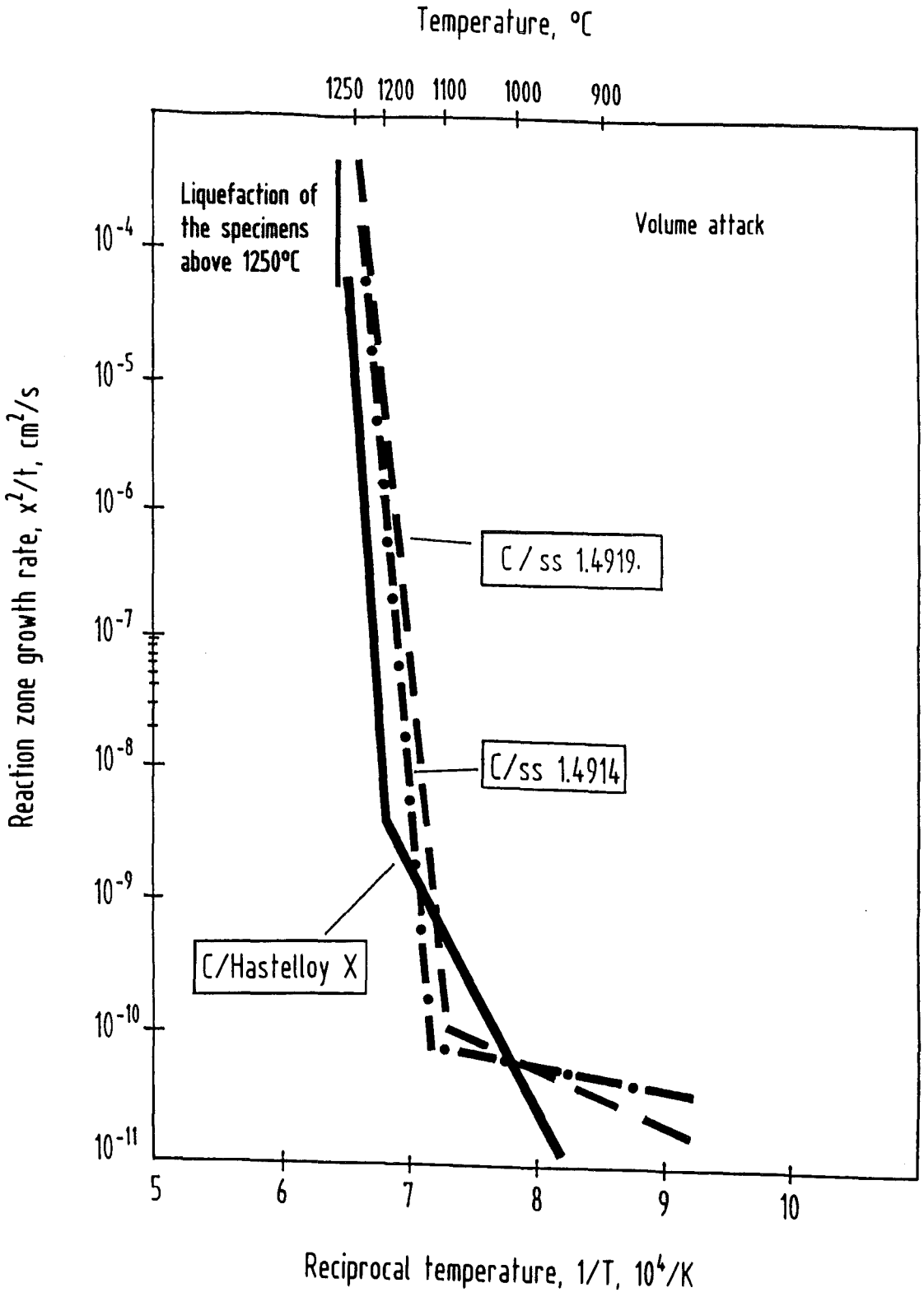

Fig. 26: Comparison of the reaction zone growth rates for the C/1.4914 ferritic steel, C/1.4919 stainless steel and C/Hastelloy X systems.